
# NAVAL POSTGRADUATE SCHOOL

**MONTEREY, CALIFORNIA**

# THESIS

**CORROSION AND WEAR RESISTANCE OF DUAL-REINFORCED AL-7075 COLD SPRAYED COATINGS**

by

Nathan E. Mathes

June 2023

Thesis Advisor: Troy Ansell
Second Reader: Young W. Kwon

**Approved for public release. Distribution is unlimited.**

*This project was funded in part by the NPS Naval Research Program.*

THIS PAGE INTENTIONALLY LEFT BLANK

| REPORT DOCUMENTATION PAGE | *Form Approved OMB No. 0704-0188* |
|---|---|



| **1. AGENCY USE ONLY** *(Leave blank)* | **2. REPORT DATE** June 2023 | **3. REPORT TYPE AND DATES COVERED** Master's thesis |
|---|---|---|

| **4. TITLE AND SUBTITLE** CORROSION AND WEAR RESISTANCE OF DUAL-REINFORCED AL-7075 COLD SPRAYED COATINGS | **5. FUNDING NUMBERS** RMK4Q; NPS-23-N081-A |
|---|---|
| **6. AUTHOR(S)** Nathan E. Mathes | |
| **7. PERFORMING ORGANIZATION NAME(S) AND ADDRESS(ES)** Naval Postgraduate School Monterey, CA 93943-5000 | **8. PERFORMING ORGANIZATION REPORT NUMBER** |
| **9. SPONSORING / MONITORING AGENCY NAME(S) AND ADDRESS(ES)** Office of Naval Research, Arlington, VA | **10. SPONSORING / MONITORING AGENCY REPORT NUMBER** |

**11. SUPPLEMENTARY NOTES** The views expressed in this thesis are those of the author and do not reflect the official policy or position of the Department of Defense or the U.S. Government. This project was funded in part by the NPS Naval Research Program.

| **12a. DISTRIBUTION / AVAILABILITY STATEMENT** Approved for public release. Distribution is unlimited. | **12b. DISTRIBUTION CODE** A |
|---|---|

**13. ABSTRACT (maximum 200 words)**

Cold spray coatings using nano- and micro-sized reinforcements have been recognized for their improvement of mechanical properties such as adhesion strength and hardness. Unknown at this time are the effects that reinforced coatings have on the wear and corrosion resistance of aircraft-grade aluminum. In this study, aluminum 7075 powders were reinforced with a combination of graphene-nanoplatelets (GNP) and micro-boron carbide (μB4C) at 2 and 4 vol.%. The composite powders were then cold-sprayed onto Al-7075 substrates. Optical and scanning electron microscopy were used to characterize splat structure, coating thickness, porosity, and corrosion modes. Wear testing was conducted on as-sprayed specimens from which depth, coefficient of friction (COF), and mass loss measurements were recorded. Results indicate a negative trend of vol.% reinforcement to wear resistance. The 2 vol.% μB4C sample showed the closest wear resistance to the control, improving mass loss by 3% and COF by 4%. For corrosion testing, coated samples were placed in a salt fog chamber, simulating an aggressive marine environment for up to 2000 hours. Pitting corrosion was found in all samples starting as soon as 1000 hours. The 2 vol.% μB4C sample had the least average weight gain and delamination of coating upon completion of the tests.

| **14. SUBJECT TERMS** cold spray, corrosion, tribology, dual reinforcement, boron carbide, graphene-nanoplatelets | **15. NUMBER OF PAGES** 85 |
|---|---|
| | **16. PRICE CODE** |

| **17. SECURITY CLASSIFICATION OF REPORT** | **18. SECURITY CLASSIFICATION OF THIS PAGE** | **19. SECURITY CLASSIFICATION OF ABSTRACT** | **20. LIMITATION OF ABSTRACT** |
|---|---|---|---|
| Unclassified | Unclassified | Unclassified | UU |

NSN 7540-01-280-5500

Standard Form 298 (Rev. 2-89)
Prescribed by ANSI Std. 239-18

THIS PAGE INTENTIONALLY LEFT BLANK

**Approved for public release. Distribution is unlimited.**

# CORROSION AND WEAR RESISTANCE OF DUAL-REINFORCED AL-7075 COLD SPRAYED COATINGS

Nathan E. Mathes
Ensign, United States Navy
BS, United States Merchant Marine Academy, 2022

Submitted in partial fulfillment of the
requirements for the degree of

**MASTER OF SCIENCE IN MECHANICAL ENGINEERING**

from the

**NAVAL POSTGRADUATE SCHOOL**
**June 2023**

Approved by: Troy Ansell
Advisor

Young W. Kwon
Second Reader

Brian S. Bingham
Chair, Department of Mechanical and Aerospace Engineering

THIS PAGE INTENTIONALLY LEFT BLANK

# ABSTRACT

Cold spray coatings using nano- and micro-sized reinforcements have been recognized for their improvement of mechanical properties such as adhesion strength and hardness. Unknown at this time are the effects that reinforced coatings have on the wear and corrosion resistance of aircraft-grade aluminum. In this study, aluminum 7075 powders were reinforced with a combination of graphene-nanoplatelets (GNP) and micro-boron carbide (μB4C) at 2 and 4 vol.%. The composite powders were then cold-sprayed onto Al-7075 substrates. Optical and scanning electron microscopy were used to characterize splat structure, coating thickness, porosity, and corrosion modes. Wear testing was conducted on as-sprayed specimens from which depth, coefficient of friction (COF), and mass loss measurements were recorded. Results indicate a negative trend of vol.% reinforcement to wear resistance. The 2 vol.% μB4C sample showed the closest wear resistance to the control, improving mass loss by 3% and COF by 4%. For corrosion testing, coated samples were placed in a salt fog chamber, simulating an aggressive marine environment for up to 2000 hours. Pitting corrosion was found in all samples starting as soon as 1000 hours. The 2 vol.% μB4C sample had the least average weight gain and delamination of coating upon completion of the tests.

THIS PAGE INTENTIONALLY LEFT BLANK

# TABLE OF CONTENTS

# LIST OF FIGURES

THIS PAGE INTENTIONALLY LEFT BLANK

# LIST OF TABLES

THIS PAGE INTENTIONALLY LEFT BLANK

# LIST OF ACRONYMS AND ABBREVIATIONS

| | |
|---|---|
| μ$B_4C$ | Micro-Boron Carbide |
| Al | Aluminum |
| CS | Cold Spray |
| GNP | Graphene Nanoparticles |
| HEBM | High Energy Ball Milling |
| MMC | Metal Matrix Composite |
| PLA | Polylactic Acid |
| SEM | Scanning Electron Microscope |

THIS PAGE INTENTIONALLY LEFT BLANK

# ACKNOWLEDGMENTS

I would like to thank my advisor, Professor Troy Ansell, for his guidance and assistance throughout my research. Also, I thank the MAE department at NPS for its overall support during this new experience. Lastly, thank you to the colleagues of room WA-204 for your mentorship, experience, and distraction during my time at NPS. I wish you luck in all your future endeavors.

THIS PAGE INTENTIONALLY LEFT BLANK

# I. MOTIVATION AND OBJECTIVES

## A. MOTIVATION AND TECHNOLOGICAL BENEFITS

The study of cold sprayed dual-nano-reinforced aluminum composite with graphene nanoplatelets (GNPs) and micro-boron carbide ($\mu B_4C$) has a limited scope of study, only having been investigated with Al coatings on a 6061-aluminum substrate. The goal of this thesis was to identify the effects that single and dual reinforced aluminum composites have when sprayed on an aircraft grade Al-7075 substrate.

Cold spray is extremely useful in marine and aerospace applications for repair and coating. The Department of Defense (DOD) is consistently seeking new ways to improve repair methods and corrosion protection within the fleet. In a military standard, MIL-STD-3021, originally written in 2008 and revised to its current state in 2019, the DOD outlines a study done on cold spray and its application to the military. The standard discusses cold spray applications for producing protective coatings, as well as performance-enhancing layers for dimensional restoration [1]. Many of the environments in which the military operates, specifically the Navy, can be extremely corrosive to the machinery, ships, and aircraft over time. A durable coating is vital to the protection of the substrate and the operation of that machinery.

A study done at the U.S. Army Research Lab in 2009 attempted to repair a number of Al-7075 helicopter mast supports which were rendered non-serviceable after mechanical and corrosive damage [2]. The study found cold spray methods with various aluminum and aluminum composite powders were successful in repairing the damaged supports. Additional research in the applications of cold spray for aircraft repair was completed by Bi et al. [3]. In this study, repair applications and mechanical properties for Al-2024 and Al-7075 were investigated to determine if cold spray could meet the regulatory requirements for basic repairs and improve properties of the substrate with coating. The repair was completed on a commonly found fastener hole which had been enlarged and worn. Implementation of cold spray in this repair was successful in fully restoring the plate to its original functional state. Additionally, the mechanical properties of the base

aluminum were found to be improved or supported by the cold spray coatings in tensile and bearing tests [3].

The aerospace industry and the DOD are always looking for improved corrosion reduction, onsite repair, and coating methods to improve the operation and safety of their equipment. Cold spray could address these needs one day and be applied as a portable system onboard military vessels for efficient and effective repair, coating, and anti-corrosion applications.

## B. OBJECTIVES OF THESIS WORK

The objective of this thesis was to investigate the characteristics of μ$B_4C$, GNP, and dual reinforced aluminum powders cold-sprayed onto an aluminum 7075 substrate with the goal of improving the mechanical properties of the material. The specific objectives of this study were the following:

- investigate the characteristics of different volume percentages of reinforcement
- improve wear resistance
- improve corrosion resistance

To compare the effects of different amounts of reinforcement contained in the spray composition, seven different mixtures were created: Al-7075 with 2 vol.% μ$B_4C$, Al-7075 with 2 vol.% GNPs, Al-7075 with 1 vol.% μ$B_4C$ and 1 vol.% GNPs, Al-7075 with 4 vol.% μ$B_4C$, Al-7075 with 4 vol.% GNPs, Al-7075 with 2 vol.% μ$B_4C$ and 2 vol.% GNPs, and a control powder of Al-7075. The powders were mixed in 50 g batches using high-energy ball milling (HEBM), this process reduces agglomeration of nanoparticles in the powders and sufficiently mixes the composition. The powders were then sprayed onto an Al-7075 substrate using identical spray parameters for each. Further discussion of the cold spray process and the effect of each parameter is discussed further in Chapter II. Powder samples were analyzed using a scanning electron microscope (SEM) to identify the reinforcements within the samples prior to spraying. After spraying, samples were analyzed to confirm the

presence of the reinforcements and identify key characteristics in the spray layers using optical microscopy and SEM.

Wear resistance was tested using a tribometer that examined and recorded the coefficient of friction and depth of wear over time. Additionally, the volume lost during the test was recorded for each sample. These results helped to determine the effect that the reinforcements had on the coatings protective characteristics.

The improvement of corrosion resistance is an extremely important goal for cold spray coatings. Determining the coatings effect on corrosion resistance was completed by submitting the samples to a simulated aggressive 2000-hour salt environment. Using a salt fog chamber, the samples were checked on a weekly basis until the end of the experiment. During the checks, the samples were weighed to determine the effects of the salt air over time. In addition to examining the overall effect of the coatings, the tests also identified the potential improvement of the $\mu B_4C$ and GNP reinforcements on the corrosion protection of the substrate.

THIS PAGE INTENTIONALLY LEFT BLANK

# II. REVIEW OF THE STATE-OF-THE-ART

## A. BACKGROUND OF COLD SPRAY

Cold spray is an additive manufacturing process that uses rapid acceleration of solid particles to form a solid, hardened coating on the surface of the substrate. This process is one of several variants of thermal spray processes, to include plasma spray and high-velocity oxygen fuel. The benefit, however, of cold spray is its ability to maintain a relatively low gas and particle temperature in comparison to other spraying operations. By maintaining the particles in a solid state and keeping the temperatures low throughout the process, the typical side effects of oxidation, distortion, and residual stresses in the substrate can be avoided [4]. These aspects allow for the system to be used in a variety of applications that would otherwise be unreached due to the high temperatures of most spray systems. Additionally, it allows for the addition of micro and nano-sized reinforcements which would otherwise be damaged in the increased temperature of other techniques [5]. Figure 1 shows the basic flow of the low-pressure cold spray process used in the system referenced in this thesis.

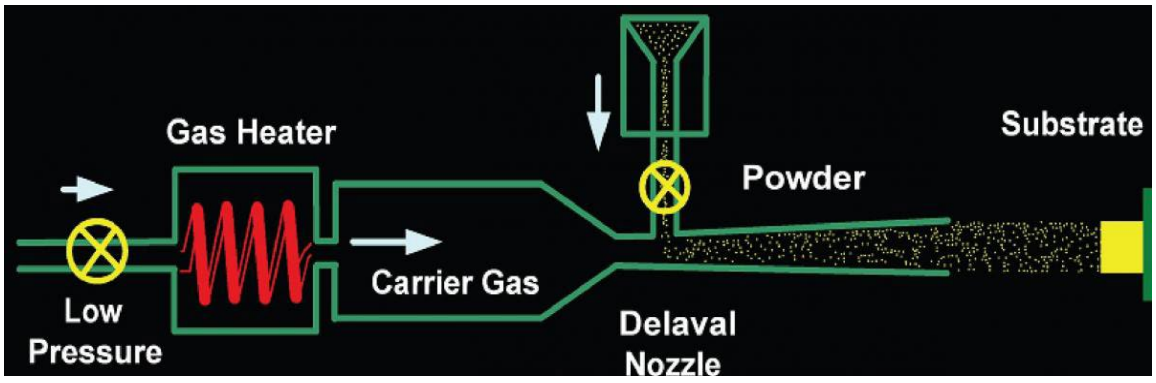


Figure 1. Basic Cold Spray Diagram. Source: [6].

## B. COLD SPRAY DETAILS

The cold spray process is achieved by use of a converging diverging nozzle or de ‘Laval nozzle which accelerates the subsonic gas and material particulates to supersonic speeds [7]. The typical metallic particles within the gas stream range from the size of 5–45 μm [4]. When the particles impact the substrate being sprayed, at velocities ranging from 450–1200 m/s, plastic deformation takes place and the particles bond to the impacted material [2]. Subsequently, the particles build up on the surface of the substrate and create a layered coating which is formed by the overlapping of splat boundaries on the material, as seen in Figure 2 [8].

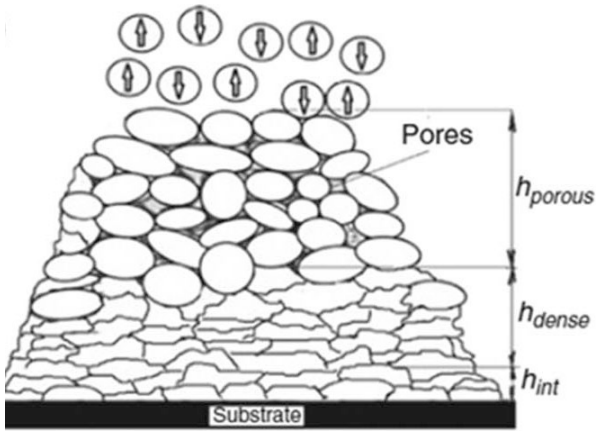


Figure 2. Splat Boundary Diagram. Adapted from [9].

Adhesion strength, as well as porosity and deposition characteristics of the coating are dictated by several factors in the spray process. These parameters are set prior to spraying and are determined by the substrate and powder materials. In order to obtain proper deposition of the particles, they must impact the substrate at a velocity higher than the critical velocity of the impacted material. This velocity value is based on the mechanical properties and morphology of the material being used [10]. Singh et al. discusses the optimization of spray parameters based on the feedstock, substrate, and other important properties [10]. Figure 3 presents the variables that are most important to the adhesion strength and therefore a proper coating.

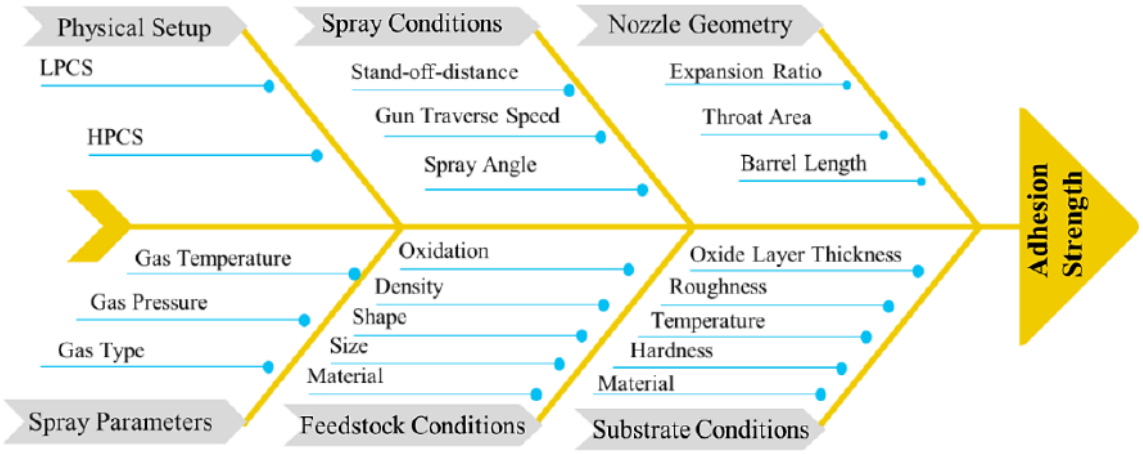


Figure 3. Adhesion Strength Parameters. Source: [10].

As seen in Figure 3, the parameters for spraying are based on many different aspects to include the physical setup (or type of system), the spray conditions, feed stock, and substrate conditions. Additionally, the carrier gas used in the cold spray operation can affect the impact velocities achieved and therefore the adhesion strength and deposition. nitrogen, helium, and compressed air are all available for use with cold spray, with nitrogen being the most common of the three due to its low cost and high availability [10]. Helium is used for specific applications due to its ability to achieve higher adhesion strengths and velocities. However, helium also contributes to higher running costs and consumption during spraying [10]. Specific to the spraying of Al-7075 on an Al-7075 substrate, proper spray parameters are limited to high pressure cold spray systems which allow for higher carrier gas pressures and temperatures. S. Ngai et al. compares the corrosion resistance of Al-7075 cold spray using both nitrogen and helium gas against a pure substrate [11]. It was found that the helium gas achieved higher corrosion resistance than was achieved with the nitrogen samples [7]. For this reason, helium was selected as the carrier gas for this thesis and the parameters were set based on parameters used by S. Ngai et al. The spray parameters used in this thesis will be discussed further in Chapter III.

## C. FACTORS THAT AFFECT ADHESION

The factors that affect adhesion strength are the same factors that are important in achieving an acceptable cold spray sample. The main area that affects the overall adhesion

of the coating is particle velocity which is determined by several parameters. The particle velocity is a main factor for achieving proper deposition on the surface of the substrate. Proper deposition is achieved when the particles deform on impact and imbed themselves in the substrate [10]. Deformation of the powder stock can be achieved when the particles attain a critical velocity. This speed can be reached with the proper optimization of spray parameters e.g., the adjustment of pressure and temperature of the carrier gas.

Higher temperatures of the carrier gas has been shown to increase the ductility of the particles, which increases bonding and deformation on impact. Additionally, higher temperatures effect the particle velocity, however, too high a temperature can negatively affect particle deposition for materials like aluminum, which can clog the nozzle [10], [12]. Like the effects of temperature, increased pressures have been found to positively affect the surface deposition of the particles. Multiple studies identified by Singh et al. [10]. showed that an increase in pressure resulted in higher energy impacts of the particles which lead to increased penetration, deposition, and bonding between the substrate-particle and particle-particle interfaces.

Particle size is the final main parameter that affects the velocity. Smaller particles (diameter > 5μm) achieve higher velocities because of their low inertia within the gas stream [13]. Larger particles are more likely to completely deflect away from the substrate due to lower velocities when compared to smaller particle [13], [14]. Although much is known of the desired characteristics for spray adhesion, parameters for an ideal adhesive coating remain generally unknown.

## D. FACTORS THAT AFFECT WEAR RESISTANCE

Wear is defined as the gradual change of a materials mass or volume which often results in the formation of loose debris [15]. Within tribology, which is the science of wear, friction and lubrication, the main factors within a material that effect wear resistance are hardness, ductility, grain size, and composition [15]. Sliding wear is the most relevant to cold spray coatings as it has a lower proportion of debris particles formed during the wear. However, abrasive wear is also possible through sliding wear if the number of debris particles involved in the wear increases [15]. The main proponent that effects the wear of

a material undergoing sliding or abrasive wear is the amount of large plastic strains, small cracks, complex loading patterns, and surface effects [15]. As the material wears, it plastically deforms and creates small loose particles which encourage further wear. During testing, the main parameters that effect wear are load, sliding speed, temperature, and sliding distance [15]. Therefore, it is important to have a consistent method for testing to ensure the data is relatable and accurate.

Specific to cold spray, coating softer substrates with harder materials exemplified by spraying Al-6061 with aluminum based bulk metallic glass (Al-BMG) drastically increased the wear resistance when compared to a pure aluminum coating [16]. However, coatings have also been seen to negatively affect the wear resistance of substrates. In Rice et al. [5], cold spray coatings with μ$B_4C$ and GNP reinforcements at 2 vol% were dry wear tested using 3 mm stainless steel balls as the counter surface. The results of these tests showed that all three reinforcements, 2% μ$B_4C$, 2% GNP, and Dual (1% μ$B_4C$/1% GNP) showed worsened cases of wear resistance when compared to the aluminum sprayed sample. This was caused by the loosened debris of the GNP and μ$B_4C$ particles which contributed to the third-body abrasives and deformation of Al particles due to sheet sliding (GNPs) [5].

## E. FACTORS THAT AFFECT CORROSION RESISTANCE

Corrosion resistance is an important factor for cold spray coatings as many CS applications require a resistance to aggressive marine environments. Aluminum cold spray coatings have been found to generally improve the corrosion performance of a substrate with better performance from coatings that see high deposition efficiencies and low porosity [11]. As identified previously, in S. Ngai et al. [11]. samples sprayed using helium gas provided much higher corrosion resistance when compared with samples sprayed using nitrogen and mixed gases. This identifies that porosity is a large factor in corrosion resistance and therefore the highest deposition density achievable should be obtained in samples.

With the addition of reinforcements to the cold spray matrix, galvanic corrosion can occur. Identified by Xie et al. [17], Al-7075 reinforced with $TiB_2$ was sprayed with

helium and air as the carrier gases. The uniformly distributed reinforcement particles caused galvanic corrosion in the as-sprayed samples. This was caused by the noble $TiB_2$ reacting with the Al matrix. Compared to the pure Al-7075 coatings, the corrosion rate was higher in the reinforced samples. However, reduced corrosion was noted on the samples sprayed using helium as opposed to air. Results from this study confirm that helium is a more efficient carrier gas for uses in corrosive applications and galvanic corrosion should be considered when using noble reinforcements such as $TiB_2$.

## F. ALUMINUM 7075

Aluminum 7075 is an alloy that is known for its desirable mechanical properties and uses in the transportation industries. The alloy has low density and a high strength to weight ratio which makes it extremely useful for aerospace applications [18]. Additionally, the specific alloy breakdown used in this thesis is identified in Table 1.

Table 1. Aluminum 7075 Alloy Powder Characteristics. Adapted from [19].

| Element (wt. %) | Al-7075 |
|---|---|
| Aluminum | Balance |
| Chromium | 0.18–0.28 |
| Copper | 1.2–2.0 |
| Iron | 0.5 Max |
| Magnesium | 2.1–2.9 |
| Manganese | 0.3 Max |
| Silicon | 0.4 Max |
| Titanium | 0.2 Max |
| Zinc | 5.1–6.1 |
| Others Total | <0.15 |

In research conducted on the combined tribological and corrosive effects on Al-7075, it was found that the limiting factors lay in its "susceptibility to localized corrosion and poor tribological properties due to its relatively low hardness" [20]. Though Al-7075 is susceptible to localized corrosion, it is possible to improve its resistance with use of MMC's.

## G. ALUMINUM 7075 METAL MATRIX COMPOSITES

Al-7075 has many desirable properties which allow for its use in numerous applications. Metal matrix composites (MMC) allow for an opportunity to further improve these desirable properties by using the base metal to accept composites as reinforcements, which subsequently have a positive effect on its mechanical properties. Al-7075 has been tested for this purpose with many different composites to include SiC, Alumina, Graphene, etc. The results of these tests found that reinforcements further increased the corrosion resistance, wear resistance, and thermal resistance of the base metal. In the same study, a comparison of corrosion resistance of pure Al-7075 to Al-7075 with $B_4C$ was discussed. The experiments found that in a sea water (NaCl) environment, pitting corrosion was observed on the pure Al-7075. However, with the addition of $B_4C$, it was found that corrosion resistance increased with higher wt.% of reinforcement.

Further success has been found with Al-7075 MMCs in cold spray. As seen by the corrosion resistance applications which were investigated in Meydanoglu et al. [21]. and mechanical properties of repaired aerospace materials investigated in Bi et al. [3]. These successes show the applications of Al-7075 in cold spray and the benefits of reinforcement for improvement of characteristics of the material.

## H. BORON CARBIDE REINFORCED COMPOSITES

Boron carbide ($\mu B_4C$) is a ceramic that is mainly used for its impressive properties with regards to temperature resistance, strength, hardness, and elastic modulus [22]. It many applications include refractory applications, abrasive powders/coatings, ballistic performance, and nuclear applications [23].

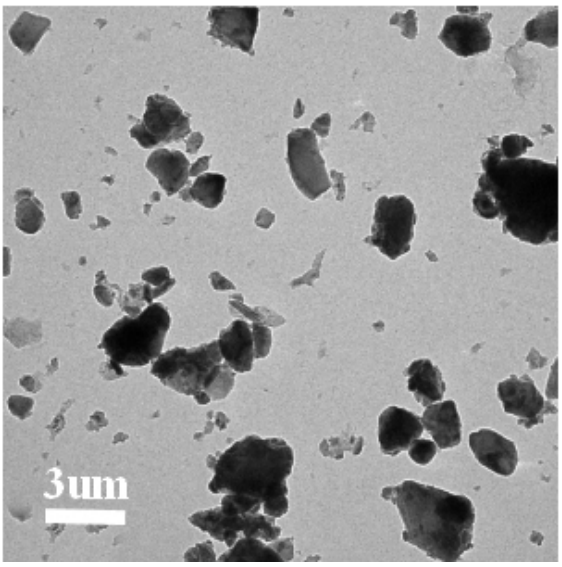


Figure 4. TEM Image of Micro Boron Carbide (μ$B_4C$) Particles. Source: [22].

μ$B_4C$ has also been found to work well as a reinforcement in metal composite matrices such as aluminum. In a study done by Nieto et al. various sizes of $B_4C$ including micrometric, submicron, and nanoparticles were dispersed in a Al-5083 matrix [24]. Hardness tests identified an increase in hardness in all samples when compared to the base aluminum with an increase in hardness as $B_4C$ particle size decreased. When wear tested, the larger $B_4C$ particles performed worse when compared to the base aluminum but the smaller nanoparticles increased the wear resistance by 7% [24]. Utilizing $B_4C$ within a MMC can be extremely useful in increasing the mechanical properties without large changes in weight or density [24].

## I. GRAPHENE-NANOPLATELETS

Graphene nanoplatelets (GNP) are made up of several layers of graphene which is a basic structural unit of graphite [5]. Single graphene layers are 0.34 nm thick, which is the atomic radius of carbon. GNPs are made up of several graphene layers which can vary from 0.7 to 100 nm in size. These layers form particles which exhibit impressive mechanical properties in addition to their light weight, and excellent thermal and electrical

conductivity [25]. GNPs have been found to work well as nanofillers within many different matrices to include many polymers, concretes, and metals [25].

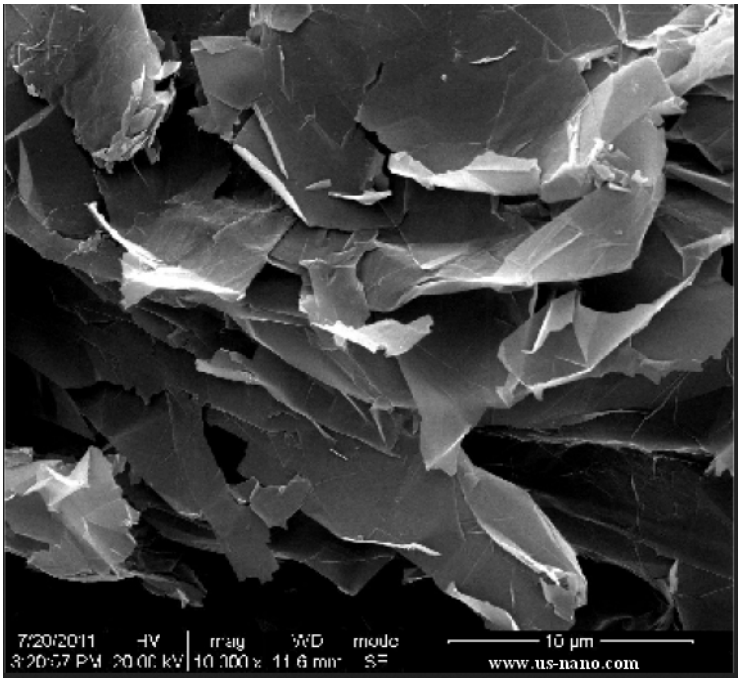


Figure 5. SEM Image of Graphene Nano-Platelets (GNP). Source: [26].

GNP reinforcement within metal matrix composites was reviewed in Nieto et al. [27]. In multiple studies, the authors found that, generally, GNP reinforcement at low vol.-% (i.e. ≤ 6.34 vol.-%) improved mechanical properties such as hardness, compressive strength, ultimate tensile strength, and flexural strength when compared to the pure Al [27]. Further, if GNPs are properly distributed throughout the Al-MMC the addition of GNPs has been found to consistently improve mechanical properties. Though it should be noted that GNP agglomeration occurs when high contents of GNPs are present [27].

THIS PAGE INTENTIONALLY LEFT BLANK

# III. EXPERIMENTAL METHODS AND MATERIALS

## A. MATERIALS AND POWDER COMPOSITIONS

The powder mixtures used in the coatings were made using the base aluminum powder and reinforcements listed in Table 2. The specific powder compositions were created following the volumetric percentages of each material in Table 3.

Table 2. Base Powder and Reinforcements.

| | Composition | Size | Density | Manufacturer |
|---|---|---|---|---|
| **Aluminum Powder** | Al-7075 | 15–53 µm | 2.81 g/cm^3 | Valimet Inc. |
| **Boron Carbide (µB$_4$C)** | µB$_4$C | 1–3 µm | 2.52 g/cm^3 | US Research Nanomaterial Inc. |
| **Graphene Nanoplatelets (GNP)** | C | 15 µm | 2.11 g/cm^3 | XG Sciences |

Table 3. Sample Compositions.

| | Powder Composition | Al-7075 [vol.-%] | µB4C [vol.-%] | GNP [vol.-%] |
|---|---|---|---|---|
| | **Al-7075** | 100 | 0 | 0 |
| **Group 1 (2% reinf.)** | **Al – GNP** | 98 | 0 | 2 |
| | **Al – µB$_4$C** | 98 | 2 | 0 |
| | **Al – GNP – µB$_4$C** | 98 | 1 | 1 |
| **Group 2 (4% reinf.)** | **Al – GNP** | 96 | 0 | 4 |
| | **Al – µB$_4$C** | 96 | 4 | 0 |
| | **Al – GNP – µB$_4$C** | 96 | 2 | 2 |

The powders were prepared using the methods outlined in the following section prior to SEM imaging. Figures 6–11 show the mixed reinforced powders as prepared for cold spray. Images taken of the spherical Al-7075 powder in Figure 6 identify the basic morphology of the powder and its make-up. Additionally, the images confirm the 5–45 µm particle sizes as advertised by the manufacturer.

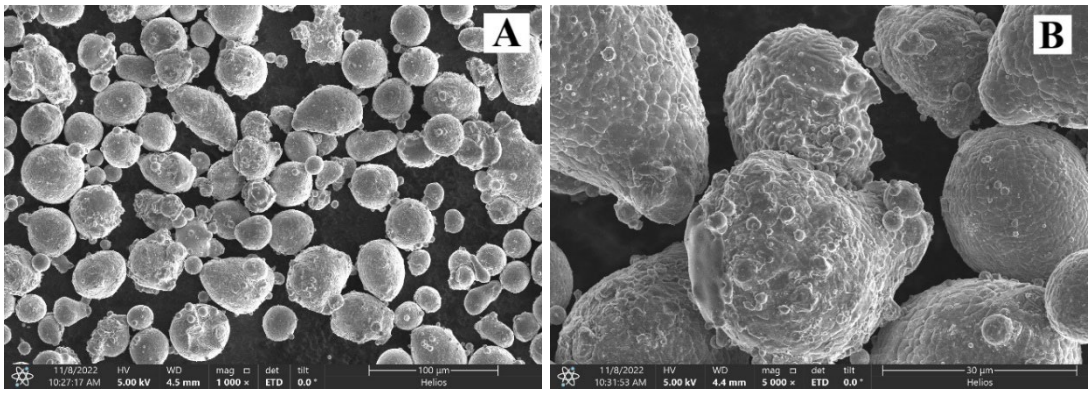


Figure 6. SEM Images of Valimet Al-7075 Powder at a) 1000x and b) 5000x Magnification.

SEM images of the µ$B_4C$ particles at 2 & 4 vol% in Figure 7 show how the µ$B_4C$ particles are attracted to the Al-7075 particles. This is seen by the reinforcements covering the surfaces of the Al particles, which shows promise for reinforcing the MMC after cold spray.

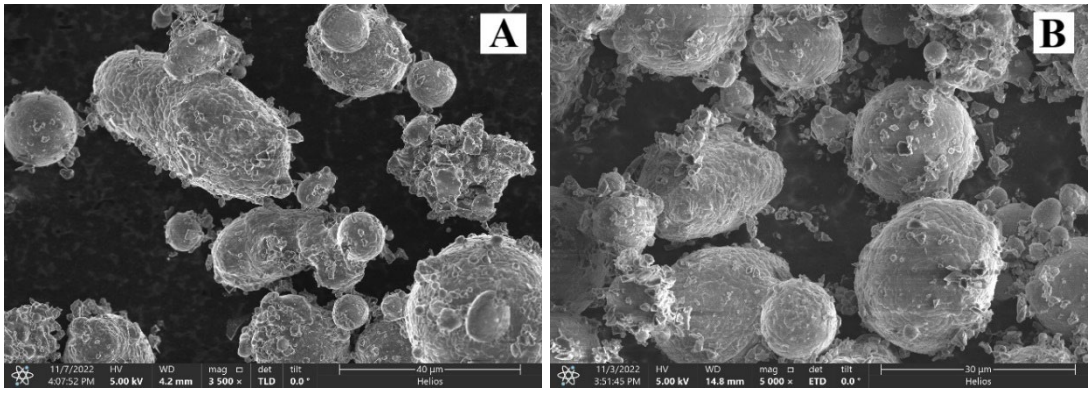


Figure 7. SEM Image of a) 2 vol.-% µ$B_4C$, and b) 4 vol.-% µ$B_4C$ Both in an Al-7075 Powder Matrix.

Like the μ$B_4C$, the GNPs are dispersed throughout the Al particles, however, tend to agglomerate into larger particles. It can be seen in Figure 8b that the greater percentage of GNPs leads to larger agglomerations in the matrix.

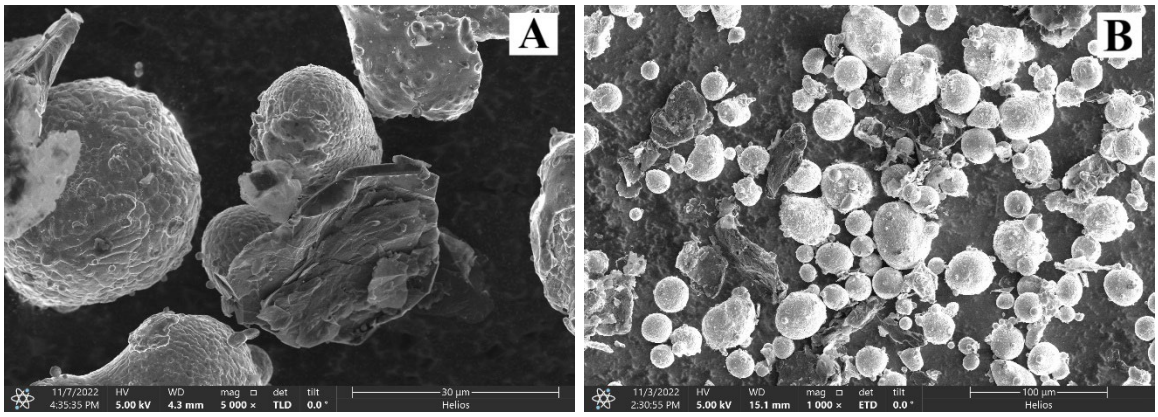


Figure 8. SEM Image of a) 2 vol.-% GNP, and b) 4 vol.-% GNP Both in an Al-7075 Powder Matrix.

The dual reinforced powders can be seen to exhibit a combination of what was seen in Figure 7 and 8. μ$B_4C$ tends to stick to the surface of the Al particles at small sizes, while the GNPs disperse themselves through the matrix at a similar size to the Al particles.

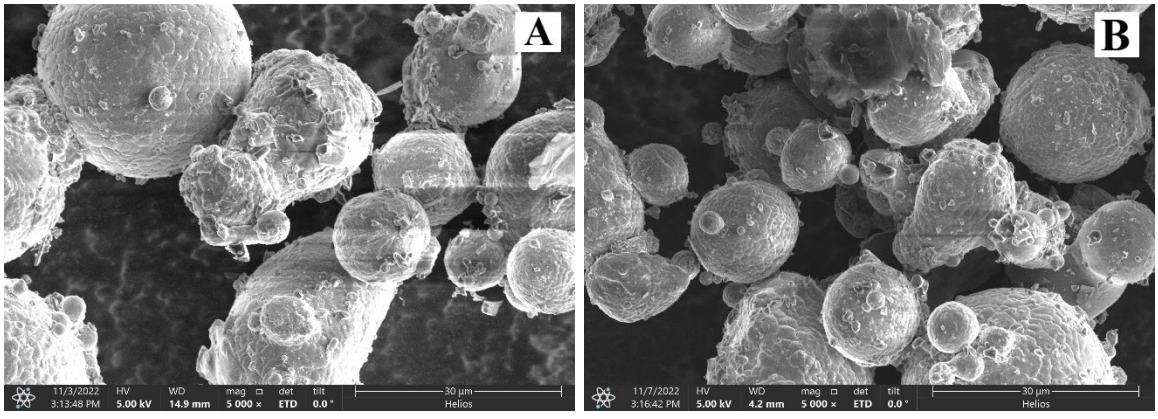


Figure 9. SEM Image of a) 2 vol.-% Dual Reinforcement, and b) 4 vol.-% Dual Reinforcement Both in an Al-7075 Powder Matrix.

## B. POWDER SAMPLE PREPARATION

Powder samples were prepared using High Energy Ball Milling (HEBM), which is a process that uses steel ball bearings as the milling media to help break up the powder particles and any agglomeration. "The HEBM is suited for powder morphology modification, grain size refinement, reactive milling, and incorporation of second phases into composite powder feedstocks" [28]. Figure 10 shows the effect that various ball to powder ratios (BPR) and cycles has on the morphology of the powder.

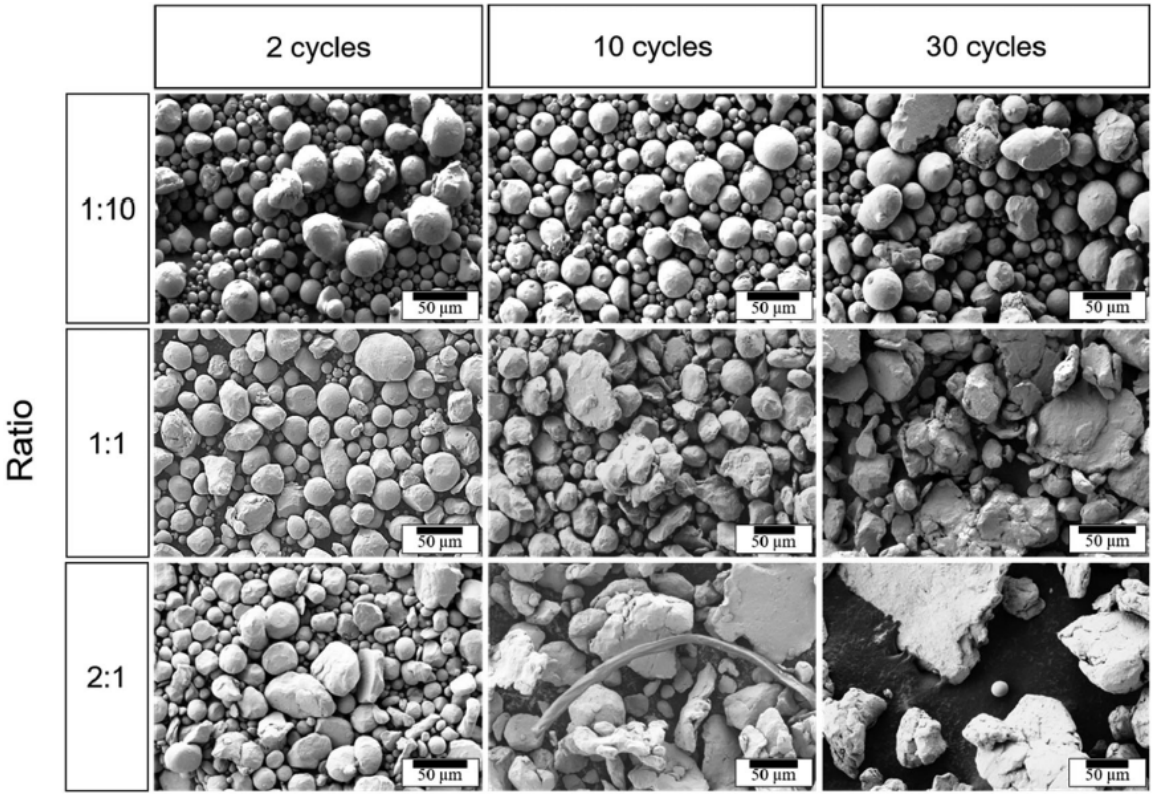


Figure 10. SEM Images of Milled 316L Stainless Steel Powders at Different BPRs and Cycles. Source: [28].

The goal of HEBM for the application of cold spray was not to change the morphology of the powder, rather to better disperse the reinforcements within the powder mixtures. The powders in this thesis were milled using a SamplePrep 8000D Mixer/Mill

as seen in Figure 11. Based on the research done by Ansell et al. [28]. and Rice et al. [5]. the HEBM parameters listed in Table 4 were chosen for this thesis.


Figure 11. HEBM SamplePrep 8000D Mixer/Mill. Source: [29].

Table 4. HEBM Parameters.

| Total Mass of Powder | Milling Media | Containment | BPR | Run Rest Cycle | Cycle Count |
|---|---|---|---|---|---|
| 50 g | 3 mm SS balls | Stainless Steel Jar | 1:5 | 2 min on 5 min rest | 10 cycles |

## C. COLD SPRAYING

All powder mixtures were milled using the HEBM parameters referenced in Table 4 and combined in glass containers as 100 g batches. The seven glass containers were labeled and placed in a 75°C oven overnight to remove any moisture prior to spraying. The aluminum substrates were prepared using an Eastwood Benchtop Blast Cabinet which uses compressed air and an aluminum oxide blast media. Substrates were sprayed to

remove the coated layer of the aluminum plates to ensure a proper adhesive surface for the cold spray.

The cold spray equipment used to spray all samples was a Centerline Supersonic Spray Technologies division (SST) Series P Spray Machine, with an added X-Feeder, and a Series P Automatic Spray Gun. In order to achieve testable samples, it was determined that two layers of each powder should be sprayed on the substrates to increase the thickness of the coatings. The spray parameters for each sample were identical and are detailed in Table 5. As discussed in Chapter II, these spray parameters were optimized using various test sprays with Al-7075 powder and substrate. Additionally, using the limited research that has been conducted with cold spraying Al-7075 feedstock and substrates, was used to help determine a baseline, which was further expanded upon based on the capabilities of the specific system used. Table 5 represents the best achievable spray parameters that were possible with the system used.

Table 5. Cold Spray Parameters.

| **Gas** | **Feed Rate** | **Nozzle Temp.** | **Gas Press.** | **Traverse Speed** |
|---|---|---|---|---|
| Helium | 15% | 310 °C | 1.21 MPa (175 psi) | 20 mm/s |
| **Stand-off Distance** | **Line Spacing** | **Nozzle Material** | **Coating Layers** | |
| 0.5 inch | 1 mm | WC-Co | 2 | |

## D. CHARACTERIZATION

### 1. Corrosion Testing

Corrosion testing was performed using an Associated Environmental Systems MX-9204 benchtop salt spray chamber as shown in Figure 12. The chamber works by creating a fine salt mist that is provided by the atomizing nozzle within the chamber. The fog is built up within the chamber and simulates a marine environment for the samples being tested.

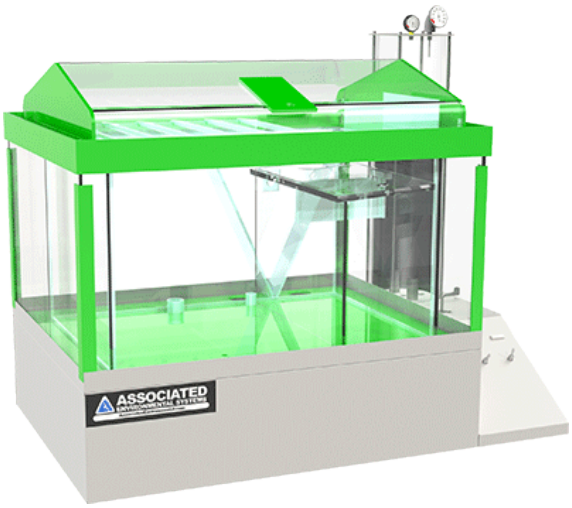


Figure 12. Benchtop MX-9204 Salt Spray Chamber. Source: [30].

The samples were placed in 3D printed sample holders as seen in Figure 13, that kept the small buildup of water from reaching the samples. These holders were printed in-house out of poly-lactic acid (PLA) by a filament fabrication method. The test was conducted for 2000 hours (12 weeks), one set of samples was removed at 6 weeks for characterization and the others were removed after the full-length of the experiment. Weights and photos were taken of the samples on a weekly basis to identify any effects of corrosion on the material.


Figure 13. Corrosion Samples in Holder Prior to Testing.

## 2. Wear Testing

Wear testing was conducted using a Nanovea T50 Tribometer, as seen in Figure 14 [31]. Using 3 mm stainless steel balls as the wear medium, the tribometer conducted a circular wear test on each specimen for one hour. Each coating sample was tested at a load of 3 Newtons, three separate times. The wear data (coefficient of friction and depth vs. time) was recorded by the tribometer and compiled into graphs to identify differences between the coatings. The wear testing parameters are consolidated in Table 6 for reference.

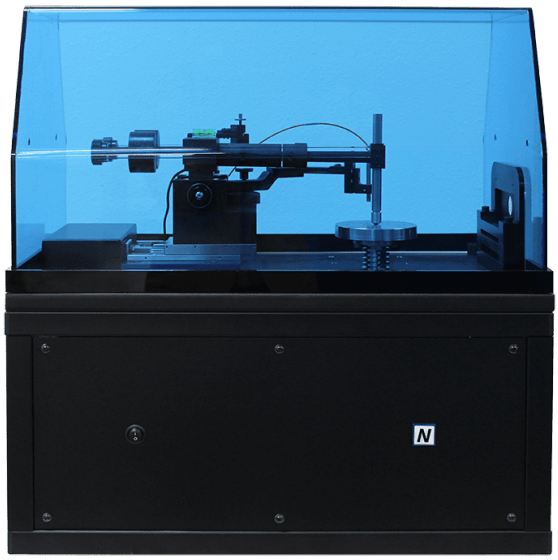

Figure 14. Nanovea T50 Tribometer. Source: [31].

Table 6. Wear Testing Parameters.

| Test Type | Load | RPM | Duration | Wear Track Diameter | Total Sliding Distance | Counter Surface |
|---|---|---|---|---|---|---|
| Orbital: ball-on-disc | 3 N | 100 | 60 min | 6 mm | 113.1 m | Ball: 3 mm SS 304 |

### 3. Sample Preparation

Samples were prepared for the various tests using a Struers Secotom-20 high speed saw, as seen in Figure 15 [32]. The original as-sprayed 3 inch samples were cut to make four corrosion samples and one microscopy characterization sample; the remainder was used for wear testing.


Figure 15. Struers Secotom-20. Source: [32].

Table 7. Sample Cutting Parameters.

| Wheel Type | RPM | Wheel Diameter | Feed Speed | Cut Distance |
|---|---|---|---|---|
| 50A20 | 2500 | 125 mm | 1.00 mm/s | 50 mm |

### 4. Microscopy Preparation

Samples were prepared for microscopy using a cold mount Struers ClaroCit, which is a fast-curing clear acrylic. The samples were then ground and polished down to a 1 µm diamond grit, as outlined in Table 8, using a Buehler Ecomet 6 grinder/polisher with 8 inch paper grinding disks and wool polishing pads. A total of three sets of samples were

prepared for microscopy using this method. Each sample underwent individual hand polishing until all prior level scratches were removed. Once every level of grit was sufficiently completed, the polished samples were placed under the optical microscope to ensure large scratches would not impede with the characterization.

Table 8. Grinding/Polishing Parameters.

| Process | Grit | Time [min] | RPM |
|---|---|---|---|
| **Grinding** | 320 | 15–20 | 350 |
| | 600 | 5–10 | 350 |
| | 1200 | 10–15 | 350 |
| **Polishing** | 6 µm Diamond | 10–15 | 350 |
| | 3 µm Diamond | 10–15 | 350 |
| | 1 µm Diamond | 10–15 | 350 |

Samples that were characterized for splat boundary and coating thickness measurements were etched using a process adapted from [5]. This was completed by using Keller's reagent which is a mixture of 2.5% nitric acid, 1.5% hydrochloric acid, and 1.0% hydrofluoric acid in water by volume. This reagent was applied to the surface of the samples to corrode the grain boundaries and allow for better characterization of the splat area.

The prepared samples were characterized under a Thermo-Fisher Helios 5-UX SEM. The samples were connected to the mounting stud using copper tape to increase conductivity. Samples were examined at various locations on the sample to obtain the best possible images of splat boundaries, surfaces, and corrosion pitting. Images from this process are investigated in Chapter IV.

### 5. Porosity Measurements

As discussed in Chapter III, porosity is an essential part of any cold spray coatings viability. Porosity refers to the presence of small voids or holes within the coating and thus can be calculated using imaging programs. Programs like ImageJ, which was used in this thesis, can be used to convert SEM images into binary black and white and produce the

percentage of black to white within the coatings. This percentage represents the pixel regions of pores over the white areas of the solid coating. Higher percentages denote a higher porosity in the coatings meaning a low spraying efficiency.

THIS PAGE INTENTIONALLY LEFT BLANK

# IV. RESULTS AND DISCUSSION

## A. COATING CHARACTERIZATION

The cold spray process includes many different operational parameters that can change the characteristics of the coating. As discussed in Chapter II, parameters such as pressure, temperature, speed, powder feed rate, powder type, etc., all influence the coating effectiveness and viability. First observations found that coating surfaces can be changed based on factors such as nozzle clogging, which was caused by the spraying of one powder type after another. To help reduce this, the nozzle and powder feed tube were cleared with compressed air between the various powder types to ensure a clean spray of the new powder sample. Figure 16 shows the produced coatings which were used for the various tests in this thesis.

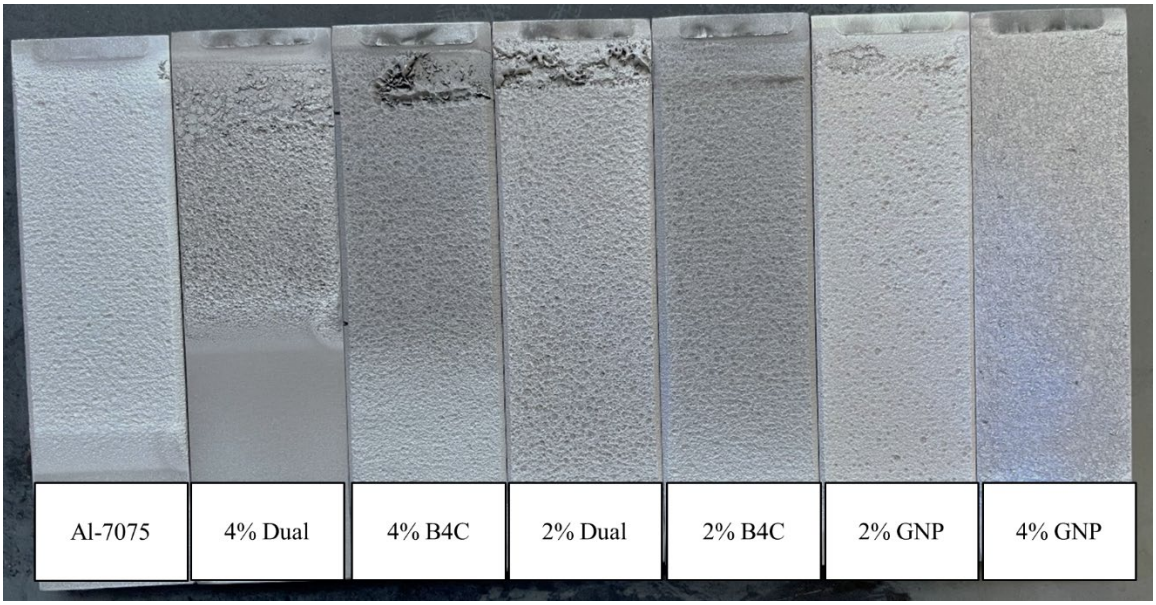


Figure 16. As-sprayed Coatings.

It should be noted that some of the coatings were more successful than others. Issues that arose were due to either running out of powder during spraying or transitioning between powders. As stated before, the powder tube was sprayed out, however, residual in

the lines still existed and caused the initial few passes to clump (as seen in the upper area of Figure 16). These areas, as well as thinned-out areas caused by low powder flow, were omitted during testing. Due to these situations, 4 vol.% μ$B_4C$ and 4 vol.% Dual, were resprayed in small sections in order to complete testing. The success of the coating is reflected in the experimental results for thickness and porosity as seen in Figure 17.

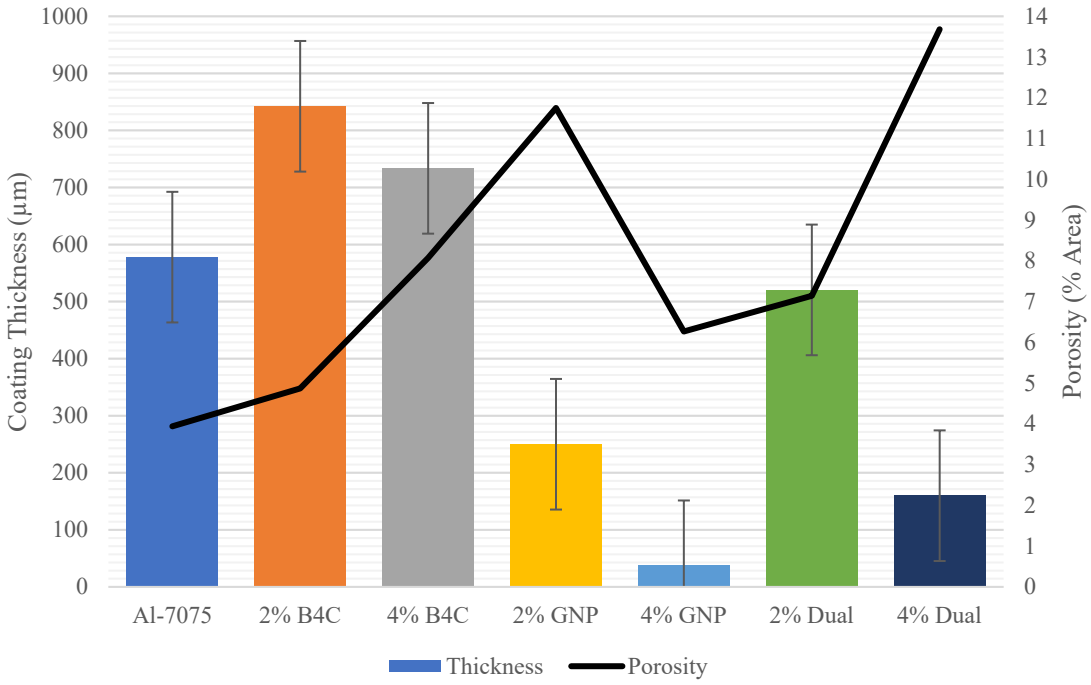


Figure 17. Average Coating Thickness and Porosity.

Figure 17 shows that the average coating thickness varies from 40 μm (unsuccessful coating due to thinness) up to 850 μm. The coatings with little to no coverage were the 4 vol.% GNP and 4 vol.% Dual concentrations, which both exhibited poor surface area coverage as well as poor substrate penetration as seen in Figure 19. Due to this, porosity measurements are based on the successful portions of the coatings and should be taken with a high level of error. Additionally, due to porosity measurements being taken based on optical microscope images, an error of ±5% should be considered for the possible inclusion of splat boundaries in the images.

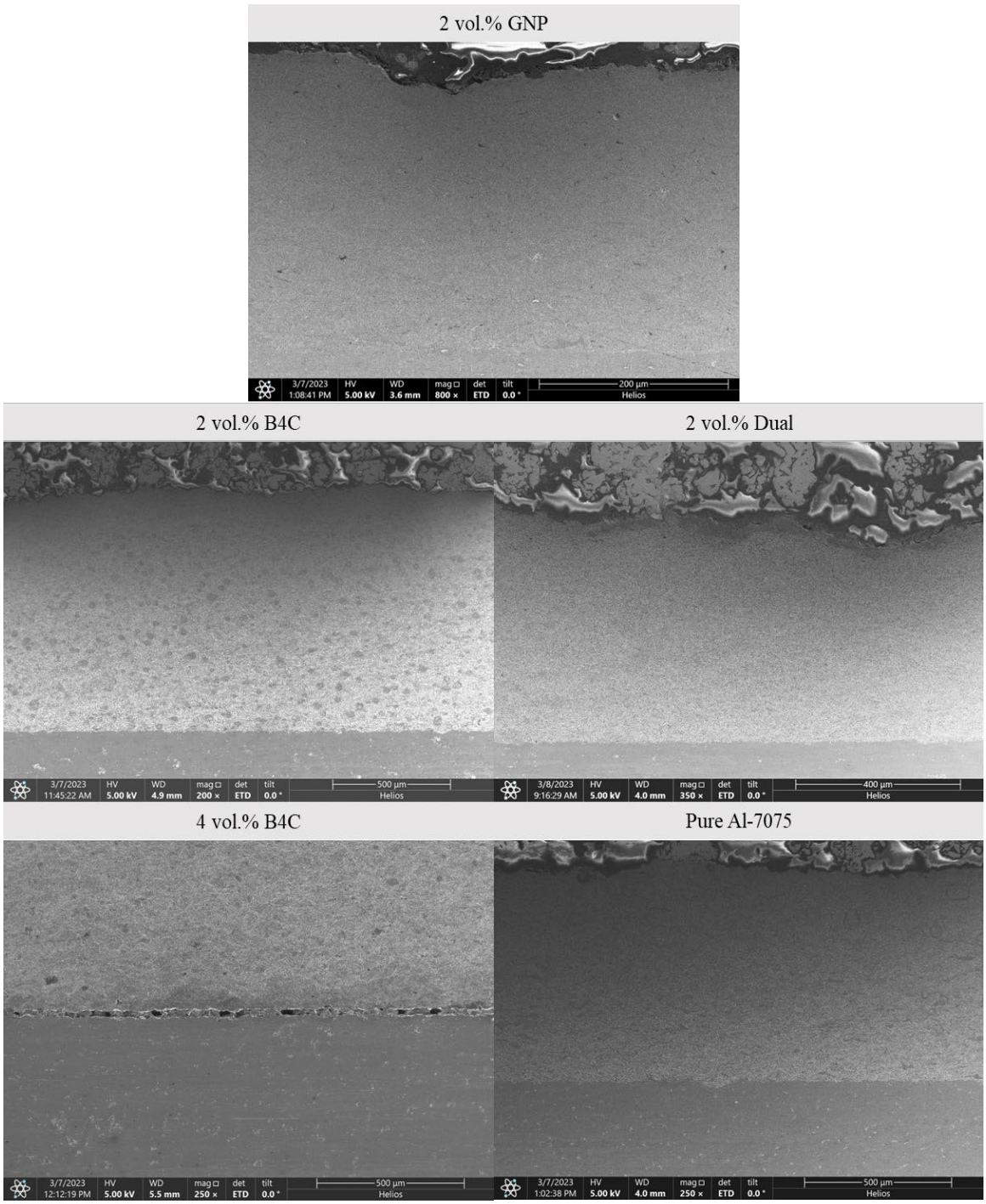


Figure 18. SEM Images of Successful As-sprayed Coating Cross-sections.

Figure 18 shows the successful coatings that were also identified in Figure 17 by their desirable thickness measurements and relatively low porosities. When compared to the base aluminum coating, the μ$B_4C$ added coating thickness as well as a slight increase in porosity.

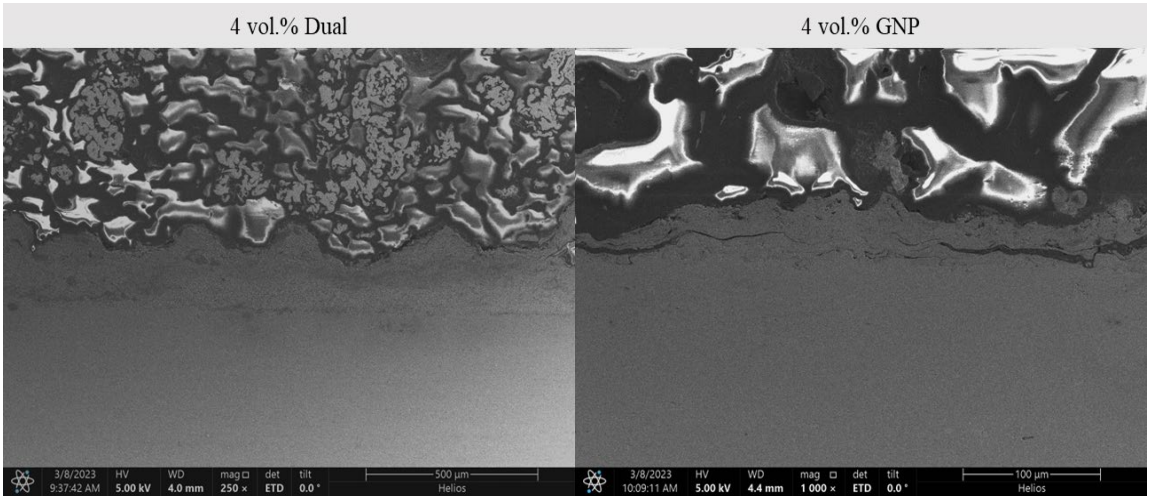


Figure 19. Coatings with Poor Deposition (high vol.% of GNP).

The coatings with poor deposition efficiency can be seen in Figure 19 and are identified in Figure 17 by their low coating thicknesses and high porosities. It is likely that a correlation exists between the vol.% of GNPs in the samples and the success of the coatings. This is due to the low density of the GNPs and their high tendency to agglomerate. The low density causes many of the GNPs to vibrate to the top of the hopper during the powder feed process. This, in combination with agglomerations in the powder matrix, can cause inconsistencies in the spray which leads to low deposition and thus high porosities. These inconsistencies are reflected in further testing of the GNP reinforced specimens later in this chapter.

Splat boundaries are identified in Figure 20 and created at the substrate and coating border. The channels that are spread throughout the image in Figure 20 were brought out by the etching process and represent the grain structure of the individual Al particles.

Figure 20a shows the splat boundary at the substrate border and Figure 20b shows a higher magnification image of the splat showing the crystal structure.

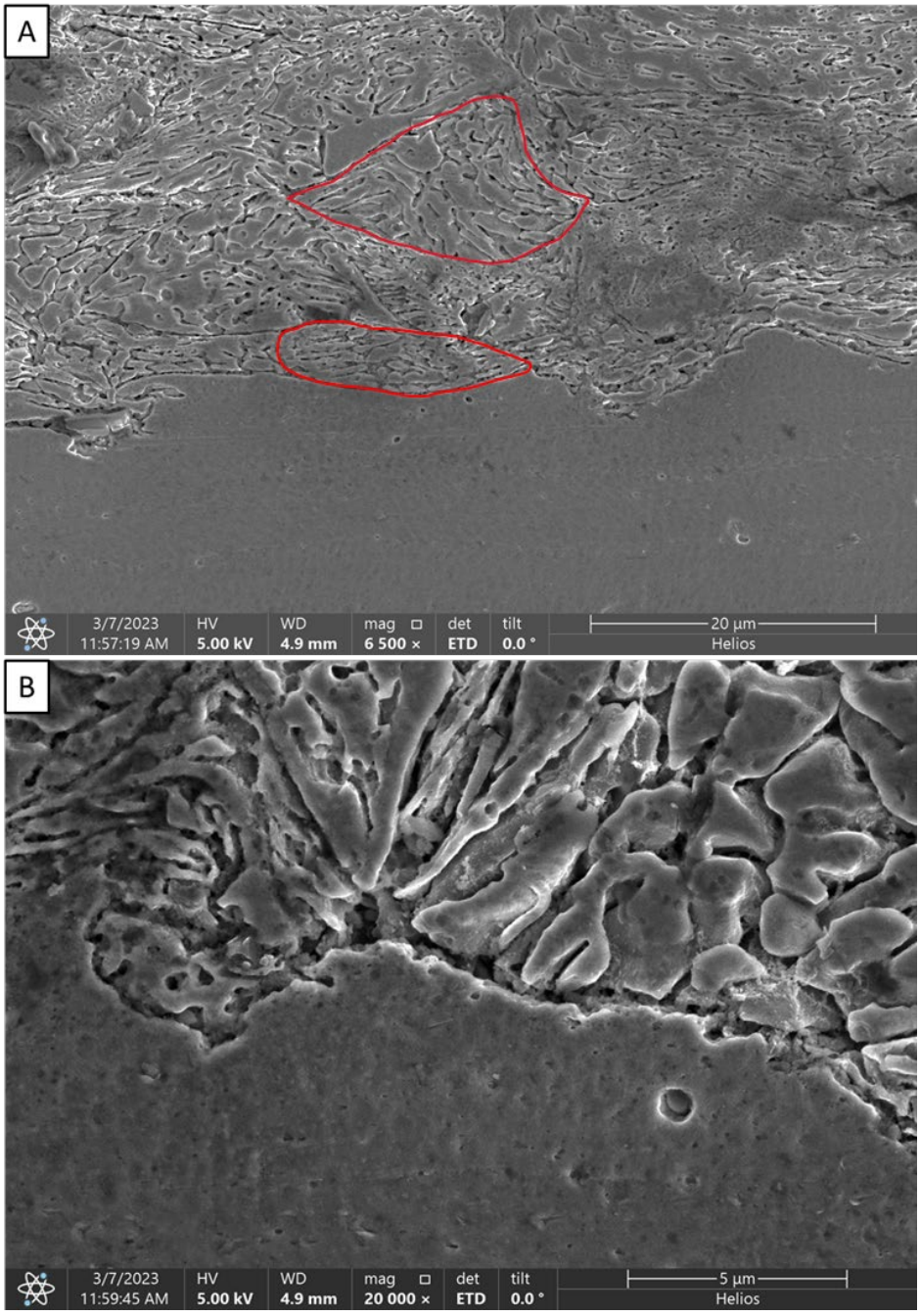


Figure 20. Coatings Showing a) Etched Cross-section of Splat Boundaries Layered in Coating and b) High Magnification of Splat Boundary at Substrate.

The substrate-coating interface in these images gives detail to the penetration at the substrate. Etched optical microscopy of the samples provide a clearer image of the splat boundaries in the coating as seen in Figure 21.

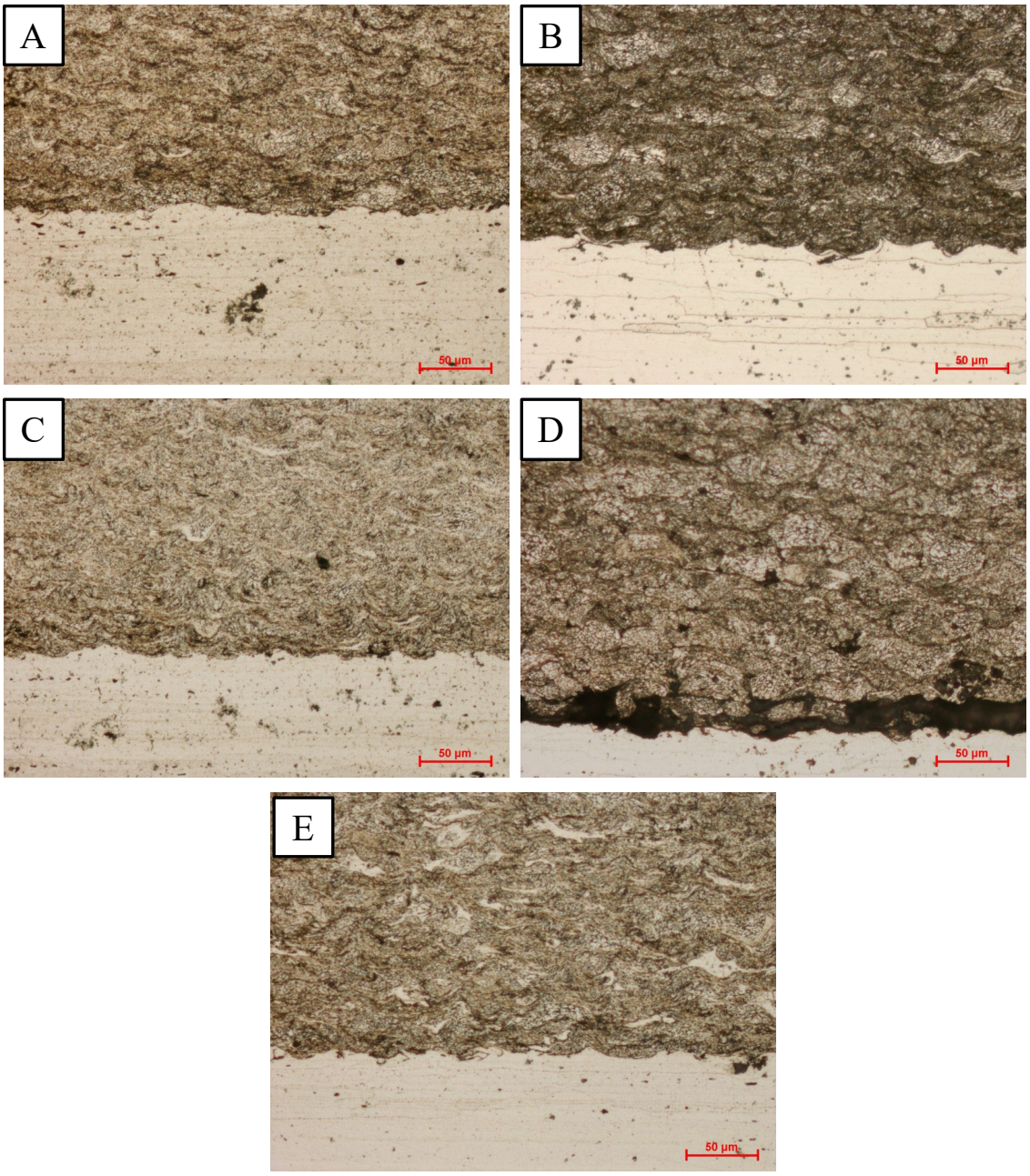


Figure 21. Brightfield Optical Microscopy at 20x of Etched a) 2 vol.% µB4C b) 2 vol.% Dual c) 2 vol.% GNP d) 4 vol.% µB4C and e) Al-7075 coatings.

The optical images in Figure 21 show the splat boundaries of the coatings with good deposition efficiency. The patterns of the splat boundaries developed during the spray process help to differentiate the coatings slightly from each other. Images 21a and 21e (2 vol.% μ$B_4C$ and Al-7075, respectively) appear to have the densest structures as the individual splats are more deformed. Image 21b, 2 vol.% GNP, appears to have a relatively dense structure, though it is not completely uniform as the splats near the substrate seem to have deformed more than the coating above it. The remaining images, 21b, 2 vol.% Dual and 21d, 4 vol.% μ$B_4C$ show splats that appear to be less deformed than what is seen with the 2 vol.% μ$B_4C$ and Al-7075 samples. The analysis of the optical images in Figure 21 confirms the porosity measurements graphed earlier in this chapter. Further, the images in Figure 22 show the cross-sections of the coatings with low deposition under brightfield optical microscopy.

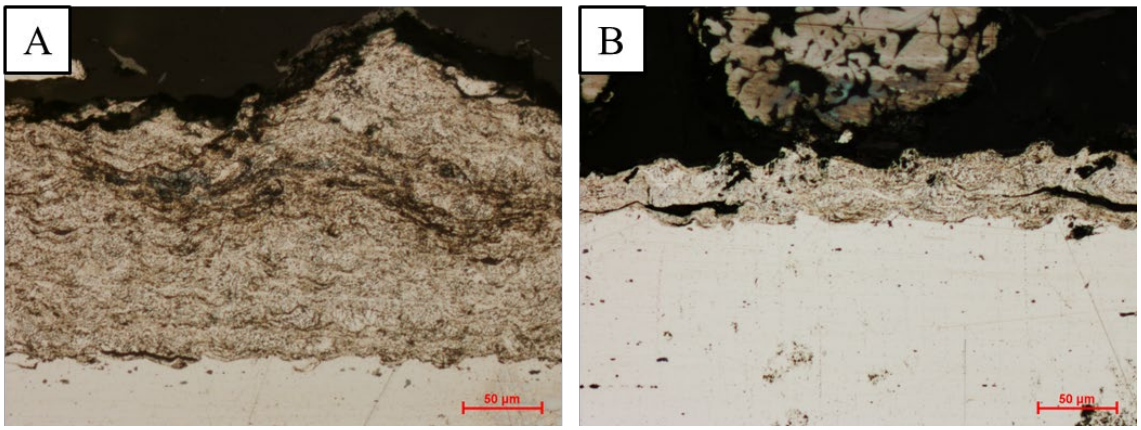


Figure 22. Brightfield Optical Microscopy at 20x of Etched a) 4 vol.% Dual and b) 4 vol.% GNP Coatings.

Figure 22 shows the poorly deposited coatings of 4 vol.% Dual (Figure 22a) and 4 vol.% GNP (Figure 22b). These images were taken at the same magnification as the coatings in Figure 21. There is a clear difference in coating thickness compared to the coatings with acceptable deposition, which was identified earlier in this chapter in Figure 17. The 4 vol.% Dual coating seems to exhibit reasonable splat boundaries near the substrate surface however, this is not consistent throughout the coating. The 4 vol.% GNP

coating seemed to have very few particles reach critical velocity, resulting in their inability to adhere to the substrate surface. This caused a minimal amount of the feed powder to penetrate and adhere to the surface and likely only resulted in the surface hardening of the substrate.

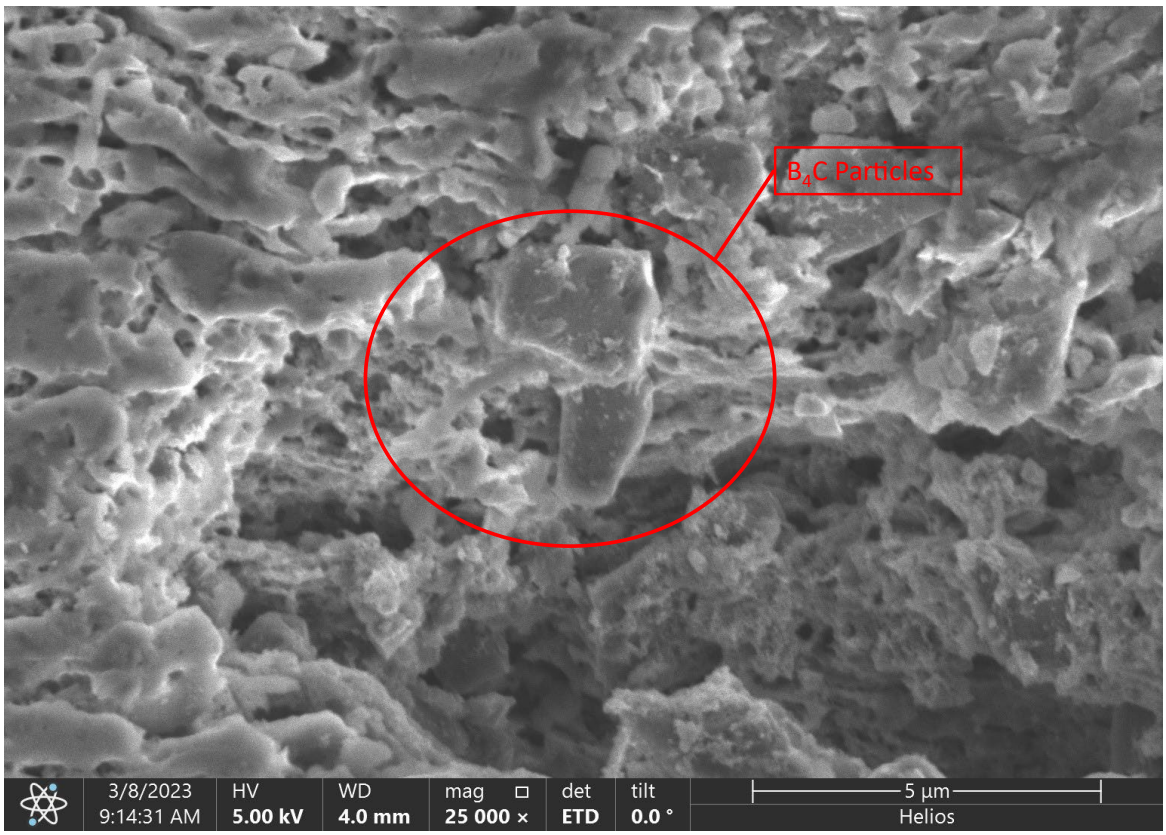


Figure 23. SEM Image of Al-µB4C Coating with Presence of µB4C Particles.

Figure 23 demonstrates the success of the µB4C coatings with the presence of µB4C particles in the as-sprayed samples. SEM images of the GNP samples were taken, however, due to the low success rate of the GNP coatings as seen in Figure 22, no GNP particles were found under the SEM. This is likely due to the GNPs poor distribution in the matrix which was further exacerbated by the consolidation of the GNPs at the top of the powder hopper during spraying (due to vibration). This would cause poor integration of the GNPs within the coating and overall poor deposition levels during spraying.

## B. CORROSION

The corrosion samples weight data was collected on a weekly basis throughout the test and compiled to show the change from week to week and the overall trend of each sample over the course of the test. The weight measurements were used as the main quantitative performance metric, while microscopy of the samples provides information on the type and method of corrosion. Figure 24 shows the average weight gain/loss across the 12-week period.

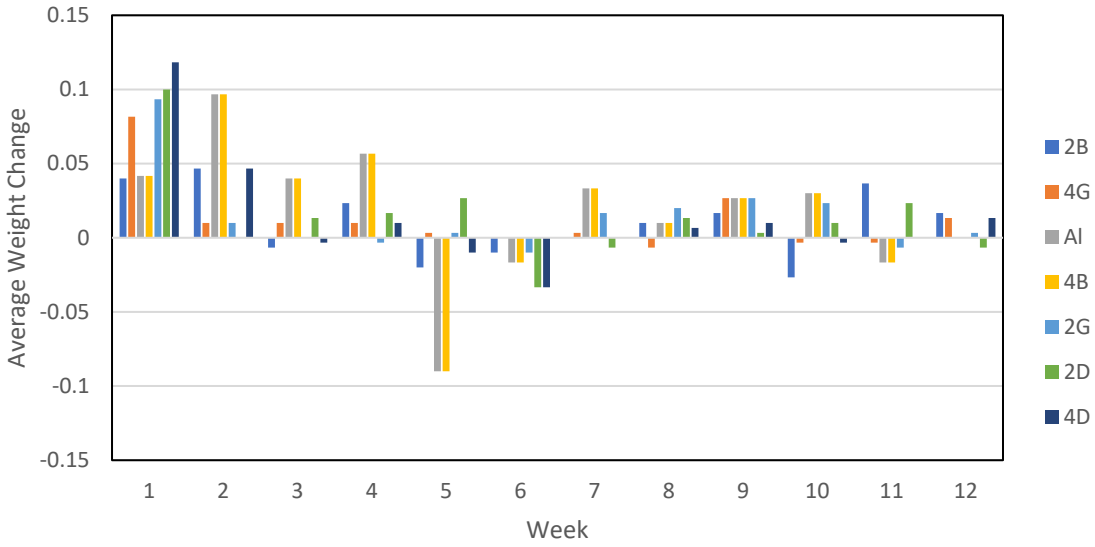


Figure 24. Average Weight Change of 12-Week Samples.

Figure 24 displays the development of the initial passivation layer in the first weeks and subsequent small weight changes that follow. It should be noted that at week 5, large salt deposits from the 4 vol.% µ$B_4C$ and Al-7075 coatings released from the samples, which caused the large loss of weight at that point. The graph shows the typical trend that is expected from the corrosion test weight data. Though, this data is not sufficient to explain the corrosion that occurred on the individual reinforced and non-reinforced coatings. Further investigation into the corrosion observed on the samples was conducted using surface and cross-sectional microscopy, which was completed on an individual basis.

### 1. Al-7075 Coating

The Al-7075 coating exhibited large concentrations of salt deposits, which continued to grow throughout the testing period. Figure 25 shows the coating at the 1000 hour (Figure 25a) and 2000 hour (Figure 25b) marks. As seen in the image, at 6 weeks there is a large amount of buildup and discoloration on the surface of the coatings. This is exacerbated by the follow-on 6 weeks, which resulted in greater salt buildup and pitting corrosion.


Figure 25. Images of Al-7075 Showing Salt Covered Samples after a) 6 Weeks and b) 12 Weeks.

The buildup of salt seen in the images in Figure 25 is confirmed by the weight change data in Figure 26. As stated earlier in the chapter, the salt deposits released from the surface at week 5 causing the slight fluctuation in weight seen in Figure 26. The samples continued to gain weight throughout the test ending in an average weight gain of 0.212 g. This is the largest weight gain of all the samples, though is not reflective of the samples pictured in Figure 27 due to the sonication of the samples for the purpose of microscopy.

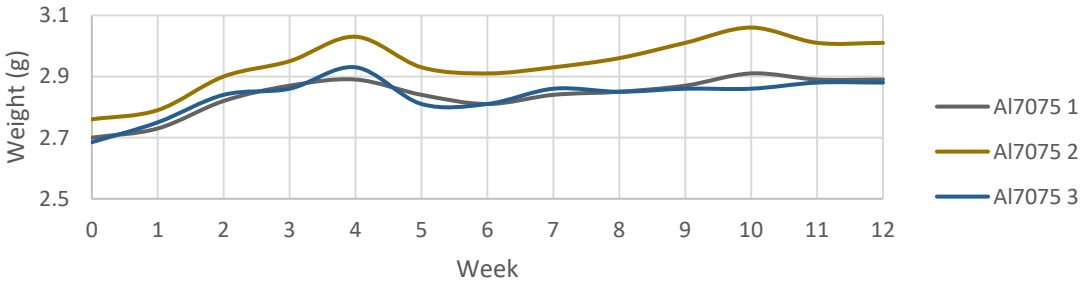


Figure 26. Al-7075 Weight Change Data during 12-Week Corrosion Test.

Further investigation of the corrosion on the coated samples was conducted by sonicating the samples to remove as many salt deposits as possible. This would allow for a clearer picture of the coating surface and any corrosive effects that had taken place. Figure 27 shows the 12-week corrosion sample after sonication.

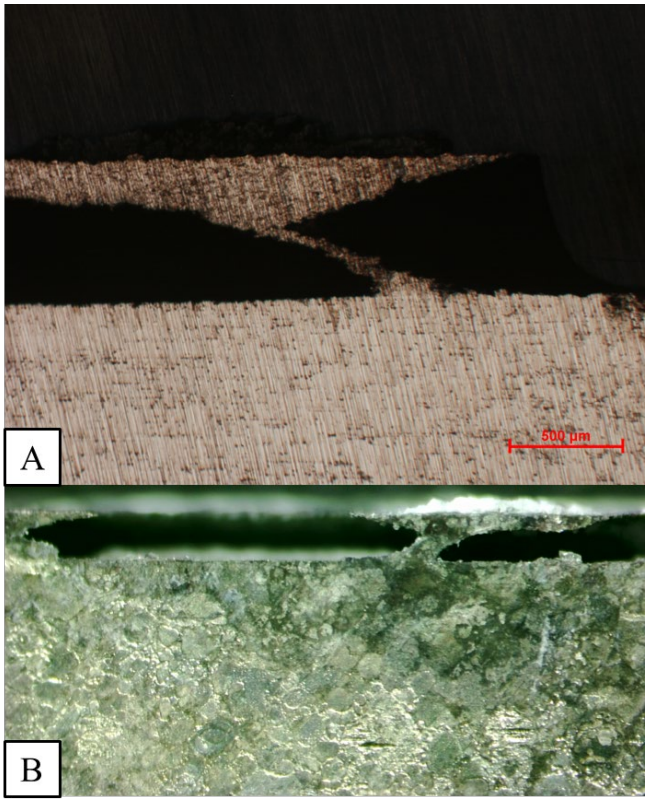


Figure 27. Al-7075 Coating Cross-sections Using a) Optical Microscopy and b) Stereo Microscopy Showing Pitting Corrosion at Substrate Boundary.

The images in Figure 27 show pitting corrosion that had propagated from the side of the sample where the coating met the substrate. The size of the pits range from less than 100 µm to up to ~400 µm. The propagation of the corrosion through the side of the coating caused the upper portion of the coating to remain intact as the corrosion spread through the sample. This caused the arch-like shape that formed on the sample seen in Figure 27. Further investigation of the samples found areas of the coating that had fully delaminated from the substrate. This can be seen in Figure 28, which shows the bare substrate area at the upper part of the image, highlighted by red.

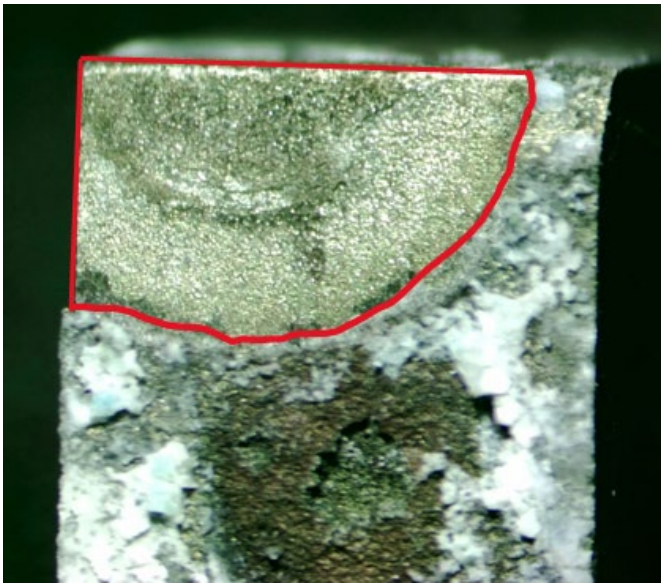

Figure 28. Al-7075 Coating Exhibiting Delamination of Coating.

The delamination of the coating from the substrate is significant and is likely caused by the cold spray process itself. Due to the high velocity of the particles impacting the surface, there is residual stress that can remain in the substrate. This stress is caused by the peening of the substrate surface during spraying [33]. This can present a weak point in the coating/substrate boundary that can be worsened in a corrosive environment. Surface preparations and spray parameters can influence this residual stress and should be investigated with further research [33].

### 2. Al-μB4C Coatings

The addition of μB4C had some positive effects on the coatings resistance to corrosion to include as-sprayed thickness and resistance to delamination from the substrate. With the exception of the pitting corrosion on the side of the 4 vol.% μB4C sample as pictured in Figure 29, μB4C reinforced coatings only showed signs of pitting corrosion at the surface. Further, this corrosion spread to an average depth of ~135 μm. No delamination of the coating was found on the μB4C reinforced samples.

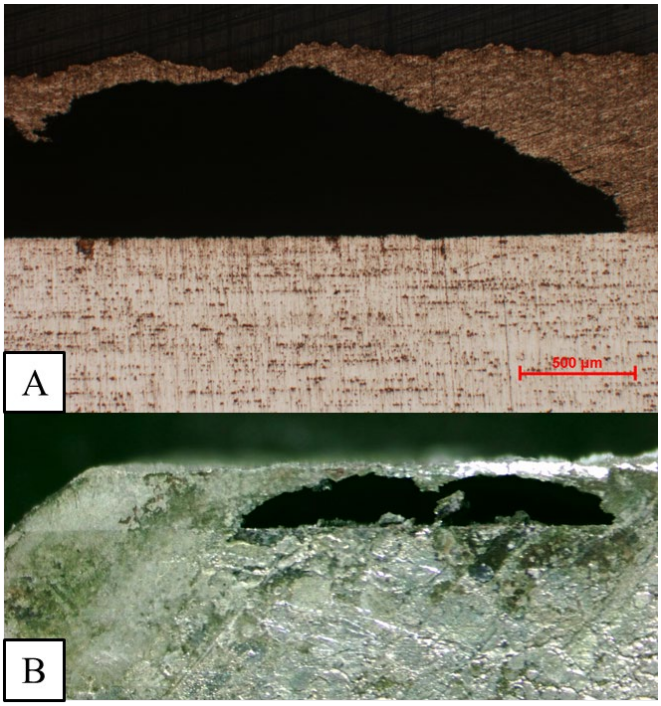


Figure 29. Pitting Corrosion at Substrate Boundary on 4 vol.% μB4C Sample Cross-section using a) Optical Microscopy and b) Stereo Microscopy.

Figure 29 shows the propagation of corrosion through the boundary between the substrate and the coating. This caused pitting at an average thickness of ~290 μm and caused a similar arch-like structure to what was seen in the Al-7075 sample. This corrosion was observed on one of the samples, though most of the corrosion occurred as the pitting corrosion seen in Figure 30.

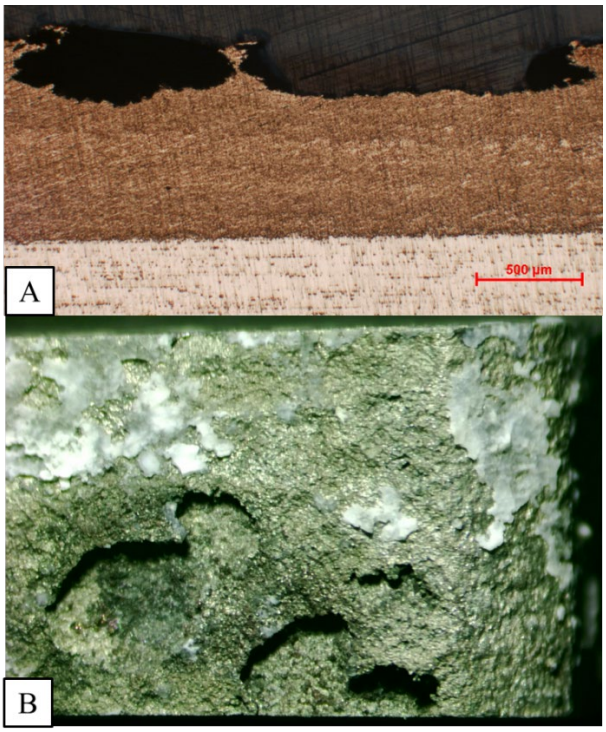


Figure 30. Surface Pitting Corrosion of 2 vol.% µB4C Using a) Cross-section Optical Microscopy and b) Surface Stereo Microscopy.

Figure 30 shows the craters that were formed from the pitting corrosion of the 2 vol.% µB4C coating. This same cratering occurred commonly on the 4 vol.% µB4C coating as well. Though, overall, the 2 vol.% µB4C coating performed well when compared to the 4 vol.% µB4C coating. The weight data in Figure 31 shows the weight change trends of the µB4C reinforced coatings over the 12-week test period.

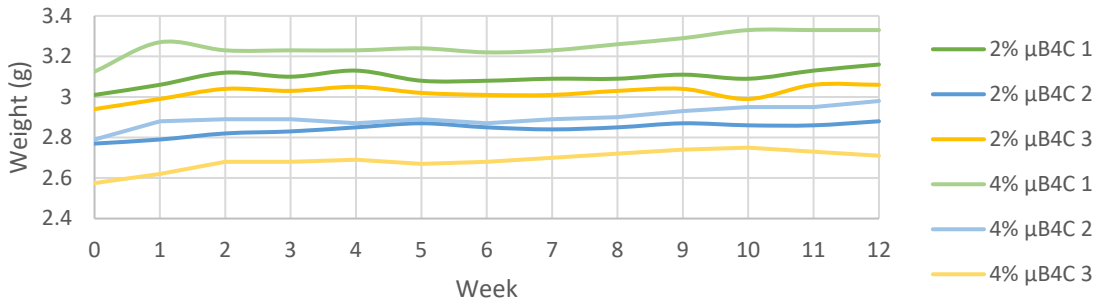


Figure 31. Weight Change Trend of µB4C-reinforced Coatings.

The average overall change across the 12 week period for the μ$B_4C$ at 2 and 4 vol.% were 0.127 g and 0.177 g, respectively. Additionally, the 2 vol.% concentration exhibited the lowest overall weight gain of all the samples across the 12 weeks.

### 3. Al-GNP Coatings

The GNP samples showed similar results to the Al-7075 sample with delamination and pitting corrosion throughout. The weight trends were as expected and can be seen in Figure 32, though the final weights found the 2 vol.% GNP to have a total average weight gain of 0.192 g. This is the second largest total gain of all the samples (second to Al-7075). The 4 vol.% GNP only gained an average of 0.145 g after 12 weeks. Though, the 4 vol.% sample was not expected to lose or gain much weight due to the thin coating.

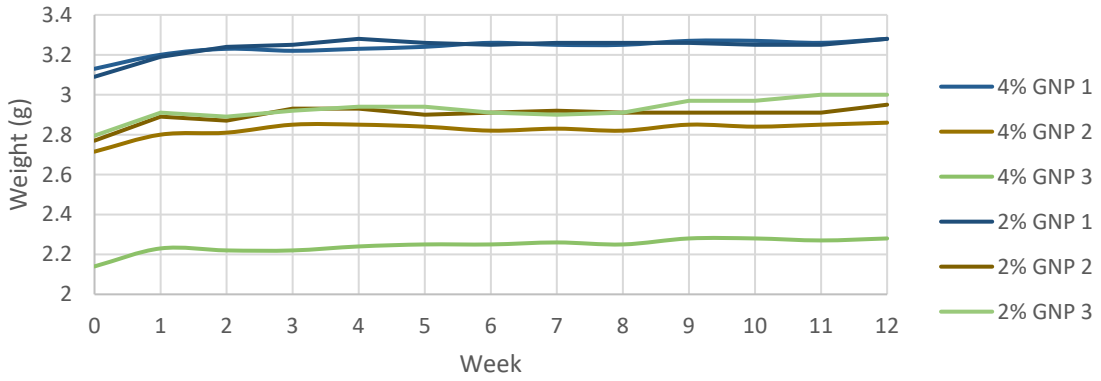


Figure 32. GNP Coatings Weight Change over 12-Week Corrosion Test.

The trends shown in Figure 32 show the weight changes of the GNP reinforced samples tested during the 12 weeks. As expected, the samples exhibit the initial weight gain in the first weeks and level off through the rest of the test. The 4 vol.% did not show any signs of severe coating corrosion during the test. However, the 2 vol.% sample showed signs as early as 3 weeks. The observed discoloration at that point spread throughout the rest of the test, Figure 33 shows the two GNP sample concentrations after 12 weeks.

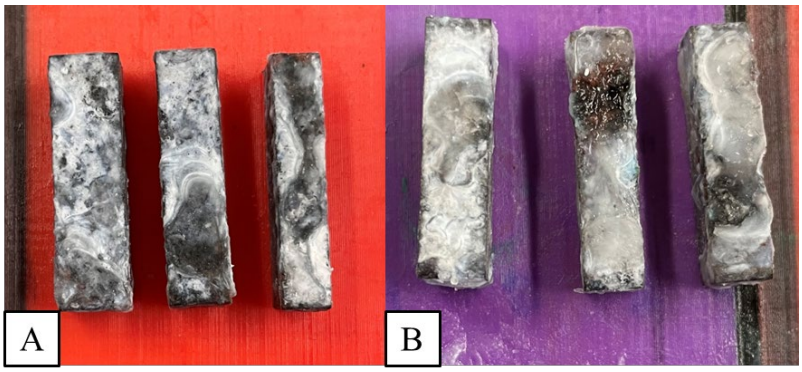


Figure 33. a) 4 vol.% and b) 2 vol.% GNP 12-Week Corrosion Test Samples.

Figure 33 shows the results of 12 weeks in the corrosion chamber and the effect on the 4 vol.% GNP (Figure 33a) and 2 vol.% GNP (Figure 33b) samples. The thin coating of the 4 vol.% GNP samples seemed to give the corrosion nothing to propagate from and therefore shows no obvious signs of corrosion. The 2 vol.% GNP samples, as stated earlier, showed discoloration and pitting which spread throughout the test. Figure 33 shows the darker sections of corrosion which caused large segments of coating to delaminate from the substrate upon sonication. The images in Figure 34 show the delamination of the coating after the 12-week corrosion test.

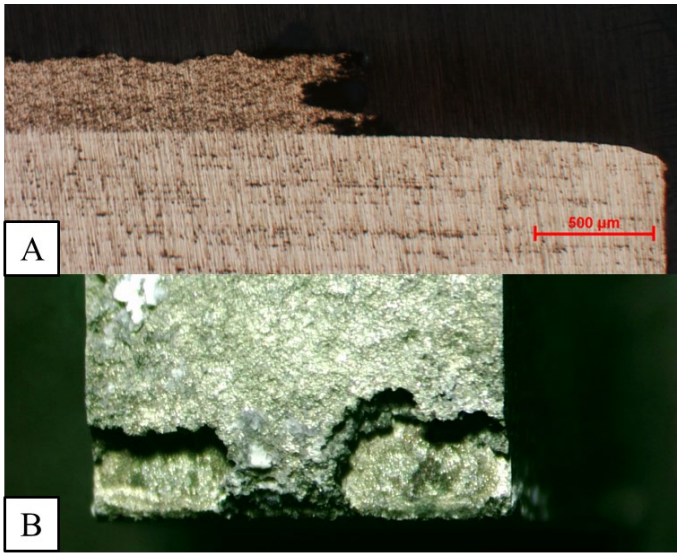


Figure 34. 2 vol.% GNP Corrosion Sample as a) Optical Microscope Cross-section and b) Surface Stereo Microscope Image.

Figure 34 shows delamination of the 2 vol.% coating from the substrate, as discussed earlier in this section. In this case, the corrosion likely propagated from the sides of the coating and in between the substrate-coating boundary. This led to a reduction in the adhesion of the coating, which caused it to delaminate during the ultrasonic cleaning process. In a similar way, the 4 vol.% was sonicated to investigate any corrosion that may have occurred under the salt layer. Figure 35 shows the 4 vol.% sample cross-section and surface after sonication.

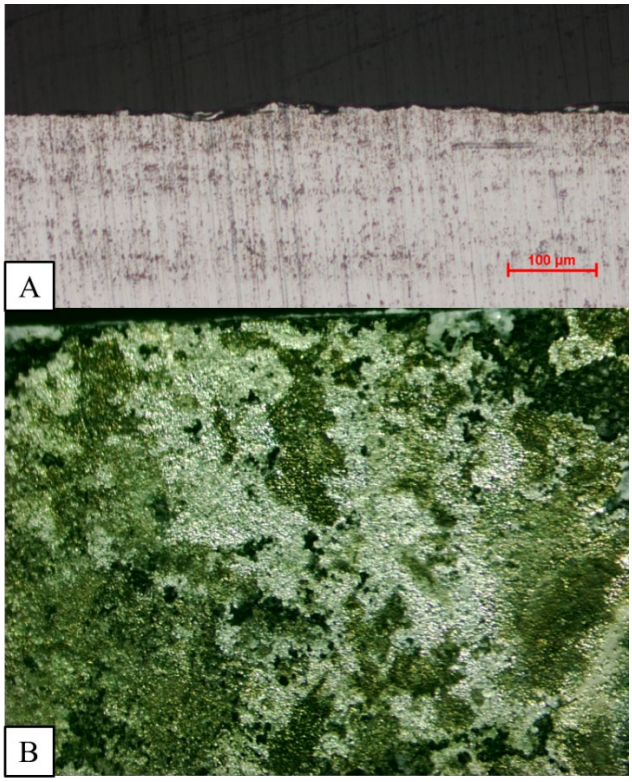


Figure 35. 4 vol.% GNP Corrosion Sample as a) Optical Microscope Cross-section and b) Stereo Microscope Surface Image.

The 4 vol.% GNP sample did not show obvious signs of corrosion during the test due to the thinness of the coatings. Upon sonication, the surface of the sample, as seen in Figure 35b, showed signs that parts of the coating had delaminated. Further investigation in the optical microscope, seen in Figure 35a, showed there were small amounts of coating left, but most had appeared to have delaminated during the corrosion test or sonication.

### 4. Al-Dual Coatings

The combination of the reinforcements in the dual coatings exemplified characteristics from both the μB4C and GNP coatings. The weight change data in Figure 36 generally follows the trend expected and seen from the other samples. The final average weight change for the dual coatings were 0.160 g for the 2 vol.% and 0.155 g for the 4 vol.%.

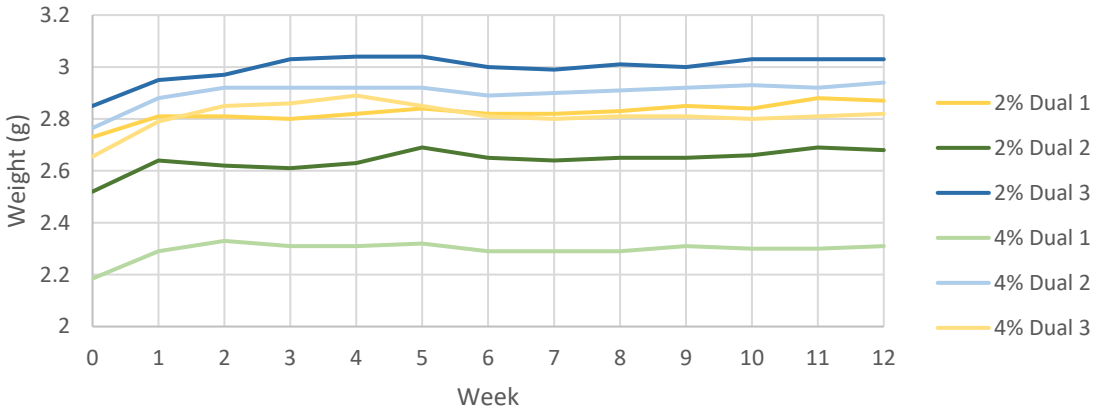


Figure 36. Weight Trends of the Dual Reinforced Corrosion Samples.

The passivation layer can be seen forming after the first week and continuing to remain for the duration of the test. The samples were sonicated to better investigate the impact of the corrosion on the samples. On visual inspection of the samples seen in Figure 37, there were obvious signs of discoloration and pitting corrosion after exposure. The samples in Figure 37 are dual reinforced samples after 12 weeks in the chamber. Both the 2 and 4 vol.% samples showed the same signs of corrosion through the discoloration and darker appearance on the surface.

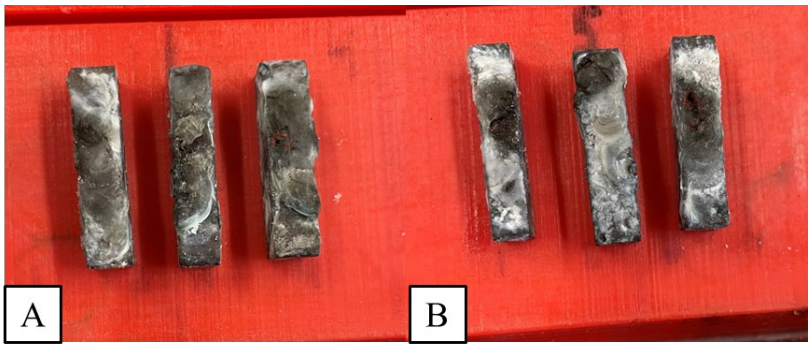


Figure 37. Dual Coating Corrosion Samples at a) 2 vol.% and b) 4 vol.% Reinforcement.

The 2 vol.% sample is shown in Figure 38 as a cross-section (Figure 38a) and surface image (Figure 38b). The cross-section shown in Figure 38a shows the pitting of the coating surface at an average depth of ~260 µm. However, much of the pitting that occurred on the sample delaminated the coating from the substrate as seen in Figure 38b. This was likely due to the same corrosion method exemplified in the other coatings earlier in this chapter.

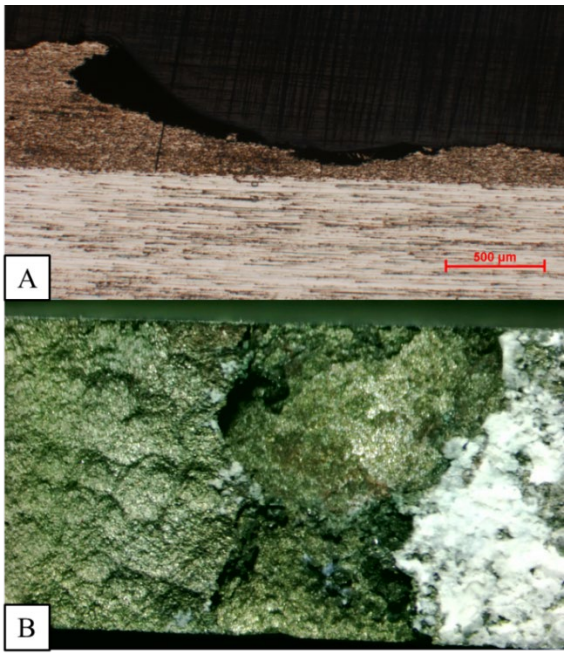


Figure 38. 2 vol.% Dual Coating Corrosion Samples as a) Optical Microscope Cross-section and b) Stereo Microscope Surface Image.

The combination of the pitting corrosion on the surface and the corrosion eating in through the side at the substrate boundary seemed to weaken the bond of the coating and caused the delamination. A similar effect was seen across a larger area on the 4 vol.% dual sample as seen in Figure 39.

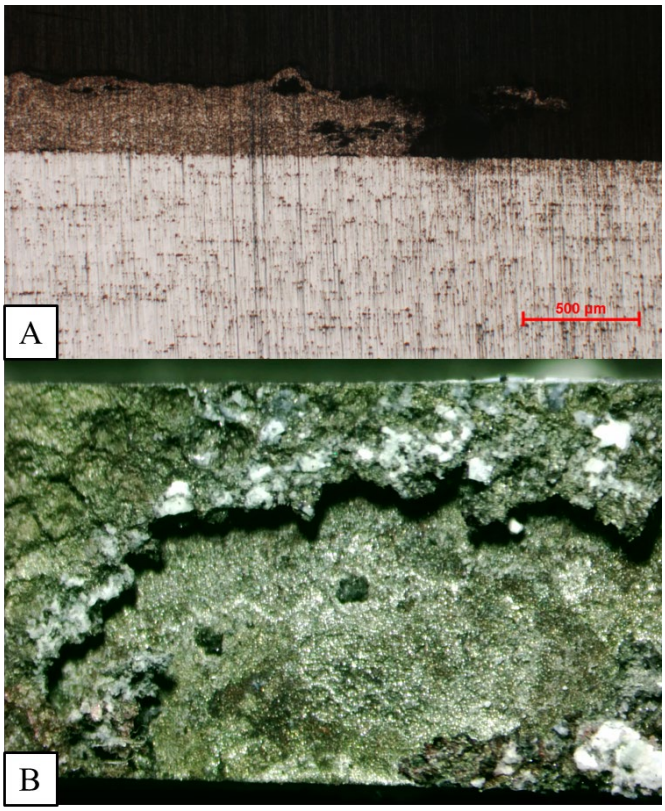


Figure 39. 4 vol.% Dual Corrosion Sample as a) Optical Microscope Cross-section and b) Stereo Microscope Surface Image.

## C. TRIBOLOGY

Wear tests were conducted in three trials and averaged across for each sample. Mass loss measurements were collected throughout testing and were compiled in Table 9. The porosities of the coatings are also included in Table 9 for reference. Al-7075 and 2 vol.% μ$B_4C$ exhibited the greatest amount of resistance to wear during testing. This is likely due to the coatings high density, which was exemplified by their low porosities of ~4% and ~5% respectively. The coating that performed the worst was the 2 vol.% GNP coating,

which had a high porosity of 11.75% for its thickness of 250 µm. This shows that although the coating had relatively high deposition, its hardness and resistance to wear were very poor.

Table 9. Wear Testing Weight Loss.

| Wear Testing Weights (g) | | | | | | |
|---|---|---|---|---|---|---|
| **Comp.** | **Test #** | **Initial** | **Final** | **Mass Loss** | **Average Mass Loss** | **Porosity (%)** |
| **4% B4C** | 1 | 11.755 | 11.7534 | 0.0016 | 0.00150 | 8.07 |
| | 2 | 11.7534 | 11.7519 | 0.0015 | | |
| | 3 | 11.7519 | 11.7505 | 0.0014 | | |
| **2% B4C** | 1 | 9.2799 | 9.2791 | 0.0008 | 0.00110 | 4.87 |
| | 2 | 9.2791 | 9.2777 | 0.0014 | | |
| | 3 | 9.2777 | 9.2766 | 0.0011 | | |
| **2% GNP** | 1 | 11.8564 | 11.8472 | 0.0092 | 0.00903 | 11.75 |
| | 2 | 11.8472 | 11.8377 | 0.0095 | | |
| | 3 | 11.8377 | 11.8293 | 0.0084 | | |
| **4% GNP** | 1 | 15.239 | 15.2354 | 0.0036 | 0.00273 | 6.27 |
| | 2 | 15.2314 | 15.2289 | 0.0025 | | |
| | 3 | 15.2289 | 15.2268 | 0.0021 | | |
| **2% Dual** | 1 | 11.7899 | 11.788 | 0.0019 | 0.00180 | 7.14 |
| | 2 | 11.788 | 11.7862 | 0.0018 | | |
| | 3 | 11.7862 | 11.7845 | 0.0017 | | |
| **4% Dual** | 1 | 10.1854 | 10.1823 | 0.0031 | 0.00210 | 13.68 |
| | 2 | 10.1823 | 10.1807 | 0.0016 | | |
| | 3 | 10.1807 | 10.1791 | 0.0016 | | |
| **Al-7075** | 1 | 23.5783 | 23.5769 | 0.0014 | 0.00113 | 3.94 |
| | 2 | 23.5769 | 23.576 | 0.0009 | | |
| | 3 | 23.576 | 23.5749 | 0.0011 | | |

The coefficient of friction (COF) was recorded throughout the tests and averaged across one hour. The original data from the wear tester was noisy and difficult to average so the data was smoothed out to better represent the COF over the course of the test. The graph of Al -7075 is included in Figure 40 for reference, graphs of the remaining samples are included in the appendix.

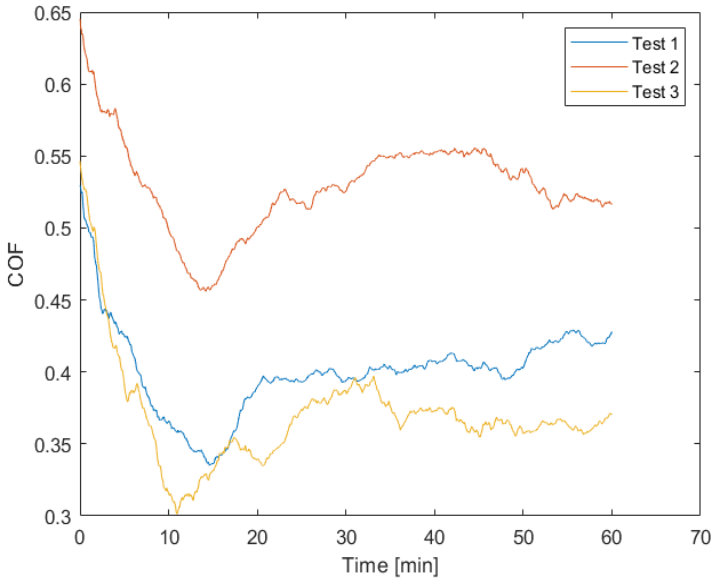


Figure 40. COF Graph of Al-7075 Wear Test.

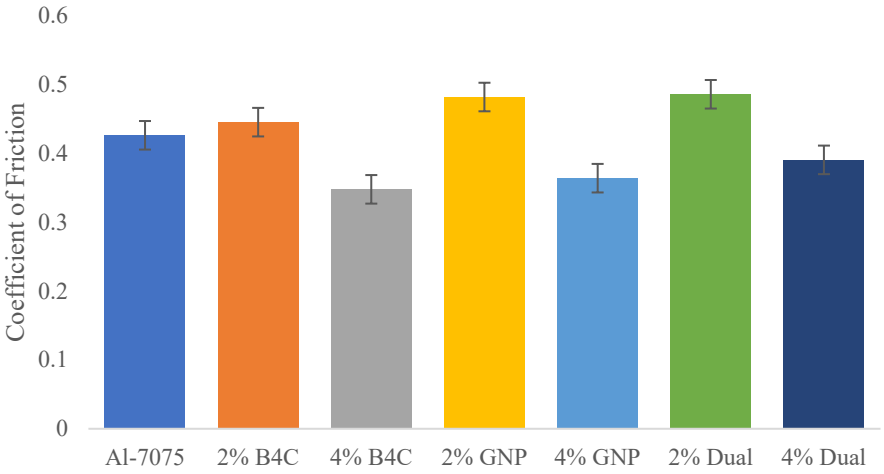


Figure 41. Average Coefficient of Friction.

The average COF data in Figure 41 was taken from the real-time graphs exemplified in Figure 40. For each test, the COF started high and gradually decreased as the surface of the coating was worn down. The first 10 minutes of wear were removed from the average to gain a more accurate average across the 1 hour test period. These COF measurements can be referenced to the surface images pictured in Figure 42.

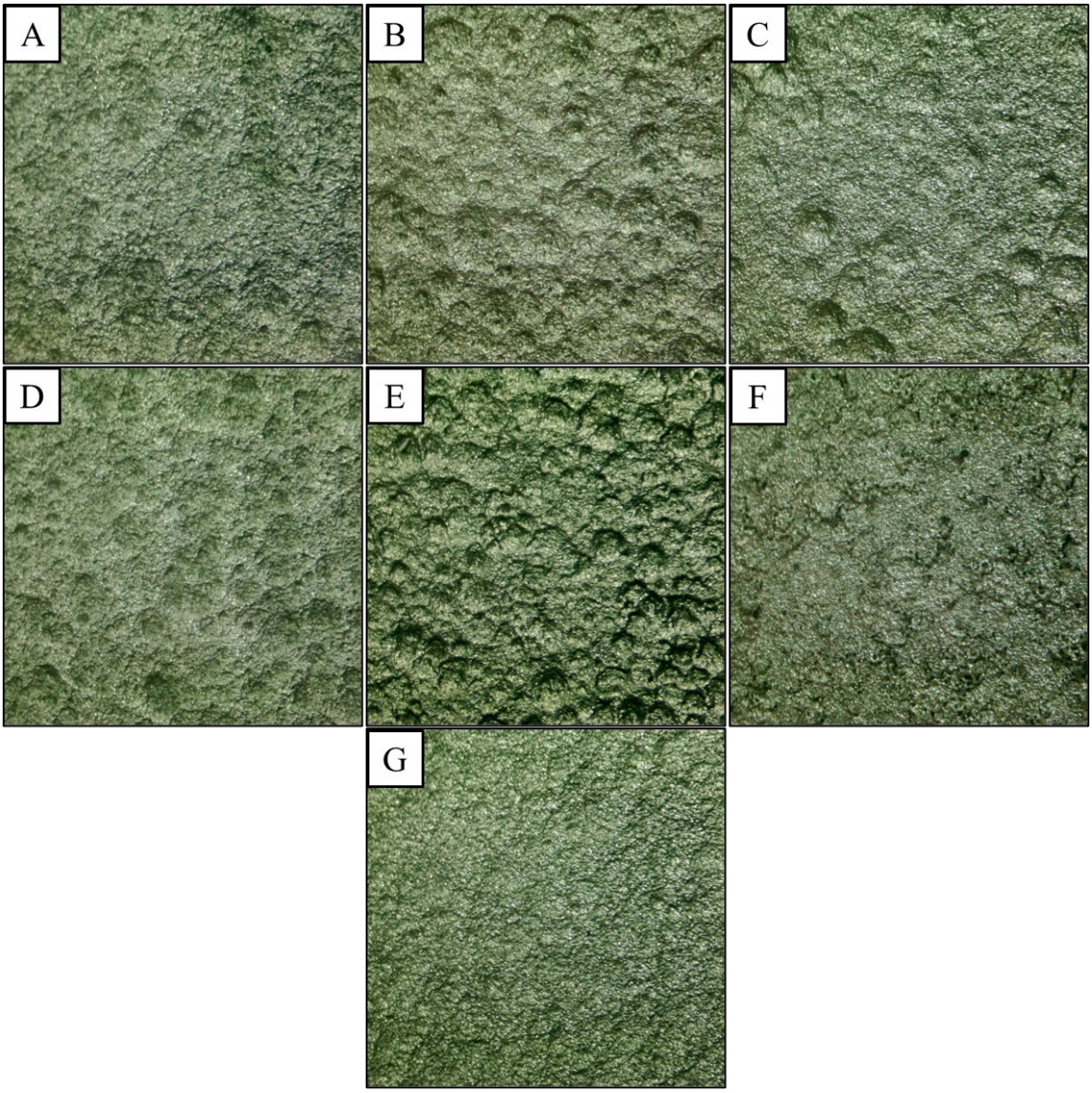


Figure 42. Coating Surface Stereo-microscope Images Identified as a) 2% $\mu B_4C$ b) 2% Dual c) 2% GNP d) 4% $\mu B_4C$ e) 4% Dual f) 4% GNP and g) Al-7075.

The images depicted in Figure 42 help to better understand the COF data collected in the wear tests. Although the surface of the specimens were worn down after the first 10 minutes of the test, the surfaces can serve as a representation of what the makeup of the coating is like. As seen in the images in Figure 42 (42d, 42e, 42f) the 4 vol.% coating samples have many deep craters on their surface, apart from the 4 vol.% GNP coating which, as stated earlier in the chapter, had very low deposition. This deep-cratered surface

shows that the coating is porous and will thus have a lower resistance to wear as compared to a smoother surface. Figure 41 gives confirmation of this as 4 vol.% $\mu B_4C$, GNP, and Dual coatings having the lowest average COFs of all the coatings at 0.3478, 0.364, and 0.3906, respectively. The other coatings showed slight improvements on the Al-7075 coatings average COF which was 0.4263. The largest improvement was the 2 vol.% Dual at 0.4859 followed by the 2 vol.% GNP at 0.4819 and the 2 vol.% $\mu B_4C$ coating at 0.4454. Overall, the surface images help to identify estimated characteristics of porosity and roughness which are in line with the results found during the wear tests.

Table 10. Specific Wear Rate for All Samples.

| Composition | Average Max Depth (µm) | Track Volume ($m^3$) | Specific Wear Rate ($m^3$/Nm) |
|---|---|---|---|
| Al-7075 | 6.2863 | 1.7551 x $10^{-9}$ | 5.1757 x $10^{-12}$ |
| 2% µB4C | 11.6986 | 6.07825 x $10^{-9}$ | 1.7924 x $10^{-11}$ |
| 4% µB4C | 10.4272 | 4.82888 x $10^{-9}$ | 1.4240 x $10^{-11}$ |
| 2% GNP | 38.3956 | 6.54744 x $10^{-8}$ | 1.9308 x $10^{-10}$ |
| 4% GNP | 29.8565 | 3.95902 x $10^{-8}$ | 1.1675 x $10^{-10}$ |
| 2% Dual | 12.8107 | 7.28881 x $10^{-9}$ | 2.1494 x $10^{-11}$ |
| 4% Dual | 9.4268 | 3.94675 x $10^{-9}$ | 1.1639 x $10^{-11}$ |

Specific wear rate, as seen in Table 10, was calculated based on the average max depth, estimated track volume, and travel distance. The standard values used for these were a travel distance of 113.035 m, a track diameter of 6 mm, and a ball diameter of 3 mm. The specific wear rate identifies the wear over the period of the test and provides a gauge for which samples performed best under the parameters set for the experiment.

The depth data was recorded by the depth encoder on the tribometer, and each test was zeroed prior to recording. The maximum depth reached was taken from the depth encoder graph seen in Figure 43 and compiled into Figure 44. The maximum depth reflects the same results that were seen with the mass loss measurements. The 2 vol.% and 4 vol.% GNP coatings showed poor wear resistance when compared to the pure Al-7075 coating

which exhibited the highest resistance to wear. The other coatings with µ$B_4C$ concentrations performed well, though as identified earlier in the chapter, the thickness of the 4 vol.% Dual coating was thin and therefore cannot be accurately measured for wear depth in comparison to its thickness.

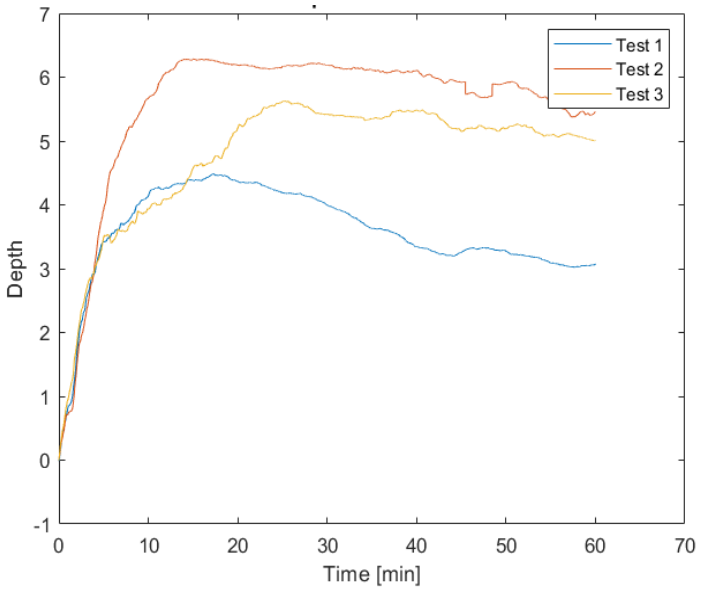


Figure 43. Graph of Depth Encoder during Al-7075 Test.

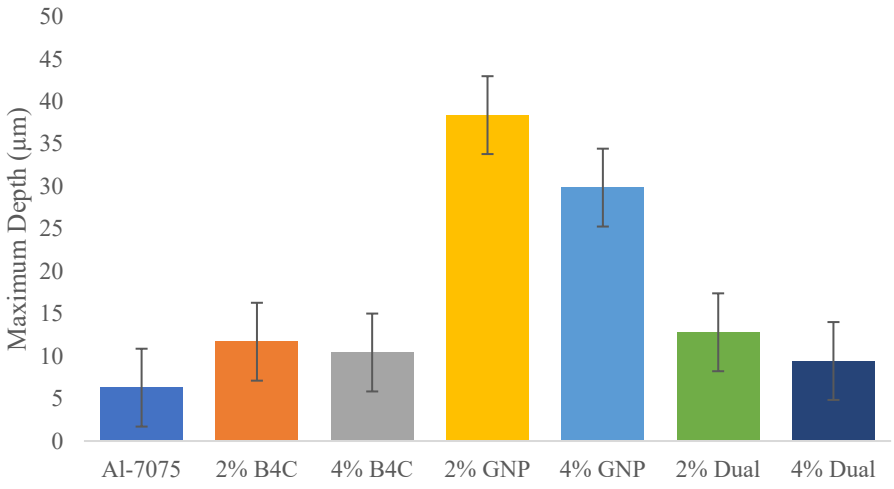


Figure 44. Maximum Depth during Wear Testing.

The addition of μB4C into the coatings negatively affected the coatings wear resistance, however, μB4C addition did lead to increases in the thickness and subsequent porosity of the coatings. The cause of the higher wear rate is likely due to the hard μB4C particles, which became abrasives throughout the test and increased the wear on the coating. This is seen through the increase in wear rate in the μB4C samples when compared to the Al-7075. The characteristics of the μB4C coatings lead to more abrasives being created, which increased wear on the thicker, but porous coatings (compared to Al-7075). Further, the 2 vol.% and 4 vol.% dual samples performed well when compared to the 2 vol.% and 4 vol.% GNP samples. The addition of the μB4C particles increased the thickness and the wear resistance of the 2 & 4 vol.% Dual coatings. In the 2 vol.% Dual coating, the synergistic effects of the reinforcements were beneficial in improving the wear resistance of the 2 vol.% GNP sample. Though when compared to the Al-7075 sample, both samples decreased overall wear resistance. Table 11 summarizes the wear test results with some other pertinent information for comparison.

Table 11. Wear Test and As-sprayed Results Summary.

| Composition | Max Depth (μm) | Average COF | Mass Loss (g) | Specific Wear Rate ($m^3$/Nm) | Thickness (μm) | Porosity (%) |
|---|---|---|---|---|---|---|
| Al-7075 | 6.2863 | 0.4263 | 0.0011 | 5.1757 x $10^{-12}$ | 577.94 | 3.94 |
| 2% μB4C | 11.6986 | 0.4454 | 0.0011 | 1.7924 x $10^{-11}$ | 842.29 | 4.871 |
| 4% μB4C | 10.4272 | 0.3478 | 0.0015 | 1.4240 x $10^{-11}$ | 733.54 | 8.074 |
| 2% GNP | 38.3956 | 0.4819 | 0.0090 | 1.9308 x $10^{-10}$ | 250 | 11.75 |
| 4% GNP | 29.8565 | 0.364 | 0.0027 | 1.1675 x $10^{-10}$ | 37 | 6.267 |
| 2% Dual | 12.8107 | 0.4859 | 0.0018 | 2.1494 x $10^{-11}$ | 520.5 | 7.144 |
| 4% Dual | 9.4268 | 0.3906 | 0.0021 | 1.1639 x $10^{-11}$ | 159.84 | 13.682 |

# V. CONCLUSIONS

The purpose of this study was to determine the effects of single and dual reinforcement in the application of low-pressure cold spray coatings. The cold spray process is a technique with many different parameters that must be in line with the materials being sprayed in order to gain proper deposition and adhesion to the substrate. Prior to spraying the samples, the parameters were tuned to find the best combination of pressure and temperature for spraying for the specific materials. Though, further investigation of these parameters is required as materials, reinforcements, and surface preparation methods can change them.

In this study, the wear resistance of the coatings was tested and indicated that the addition of μ$B_4C$ reinforcement, although increasing coating thickness when compared to the base aluminum coating, generally had a negative effect on the wear rate of the coatings. The GNP reinforced coatings performed very poorly due to their overall low deposition and high porosity. The combination of the two reinforcements in the Dual coatings performed in the middle, seeming to directly combine the negative effects of the GNP with the positives of the μ$B_4C$. Overall, the testing found the Al-7075 coating to perform the best having a combination of desirable overall thickness, porosity, and wear rate.

The corrosion tests did not reflect the same results seen in the wear tests, the Al-7075 performed poorly with the greatest average weight gain across the different concentrations and observed pitting corrosion and delamination throughout the sample. The 2 and 4 vol.% reinforced μ$B_4C$ coatings performed well with only signs of pitting corrosion on the surface and at the coating-substrate interface; with no delamination observed. The Dual and GNP reinforced samples performed very similarly, all exhibiting pitting corrosion and delamination throughout. Generally, Al-7075 is not a solution for marine environment coatings due to its susceptibility to pitting corrosion after only a short time of exposure. Though applications where Al-7075 can be used as a coating away from corrosive environments, would benefit from its desirable mechanical characteristics. This thesis serves as a guide for future research in the optimization of spray parameters, material selection, and testing procedures.

THIS PAGE INTENTIONALLY LEFT BLANK

# VI. RECOMMENDATIONS

- Spray parameters for Al-7075 powders and substrate require further optimization to achieve better deposition of the coating. Depending on the percentages of reinforcement, powder type, and mixing method, different parameters could positively effect the efficiency of the spray.
- The effects of heat treatment have been shown to positively effect the porosity of coatings. Testing this on the Al-7075 coatings in this study would be valuable in investigating the possible wear and corrosion resistance benefits from heat treatment.
- To confirm the corrosive resistance of the μ$B_4C$ coatings in this study, a corrosion test with larger samples should be completed to test the pure surface pitting corrosion without the intrusion of substrate-coating interface pitting corrosion.
- To better reduce the agglomeration of the GNP reinforcements in the MMC, other methods of mixing and separation should be investigated. Better mixing of the GNP in the powder matrix would help to keep the GNPs separated and possibly achieve better spray quality.

THIS PAGE INTENTIONALLY LEFT BLANK

# APPENDIX A: WEAR COF GRAPHS

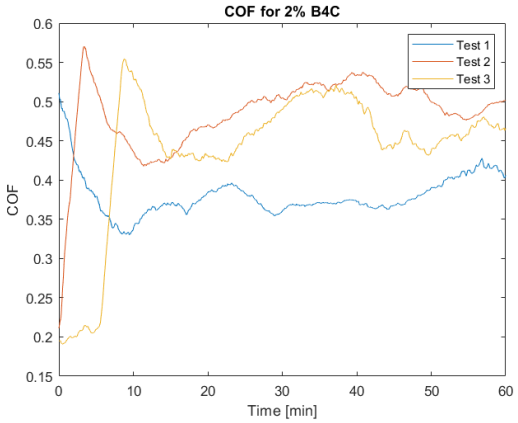


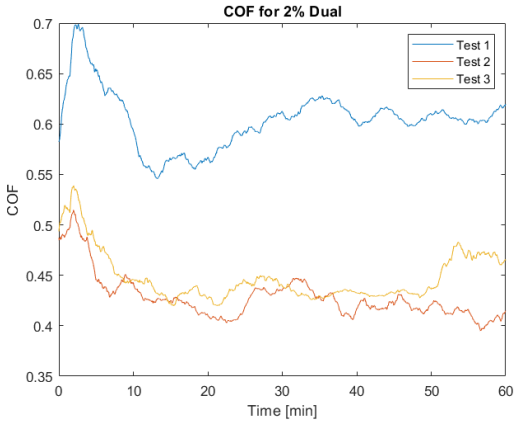


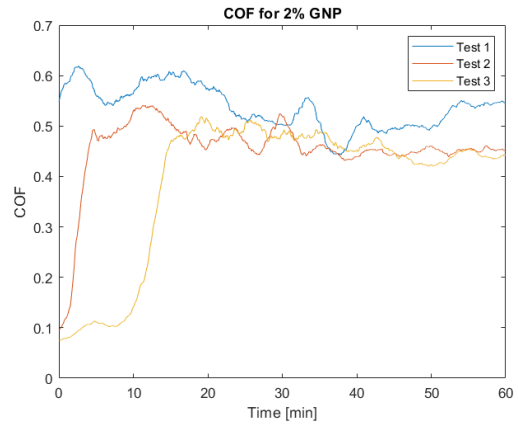


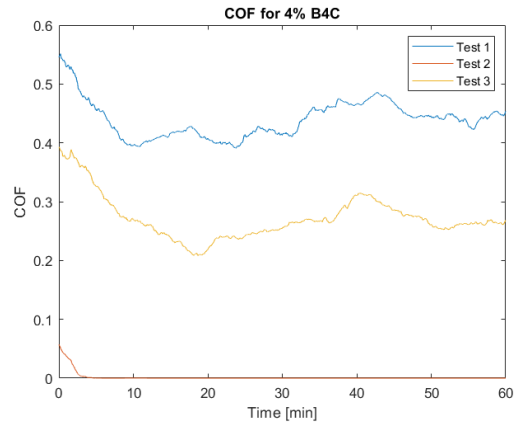


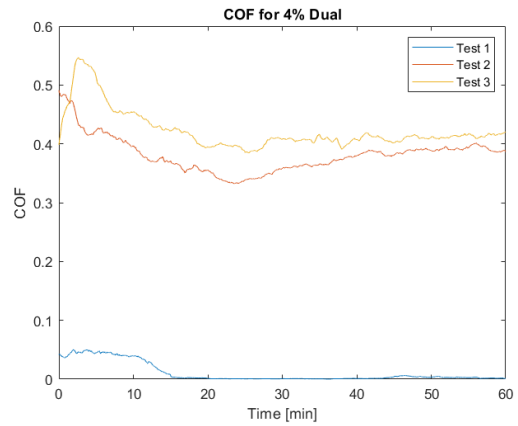


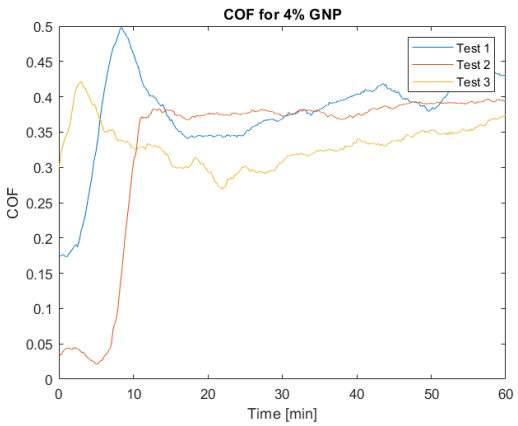

THIS PAGE INTENTIONALLY LEFT BLANK

# APPENDIX B: WEAR DEPTH GRAPHS

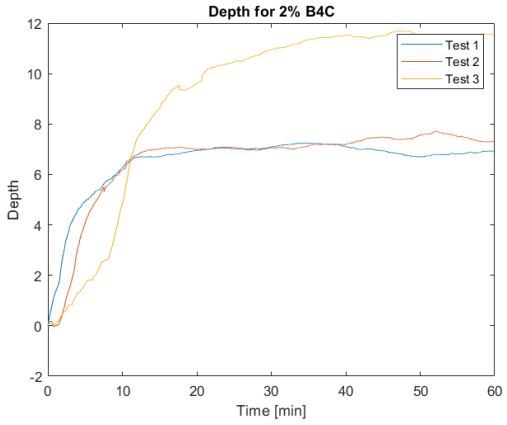


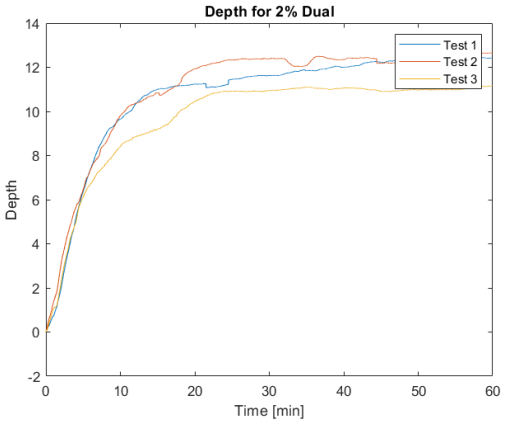


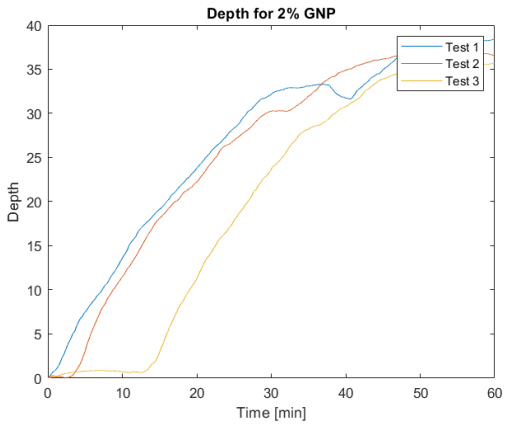


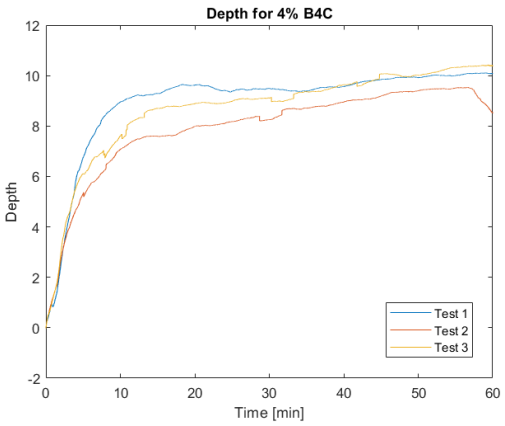


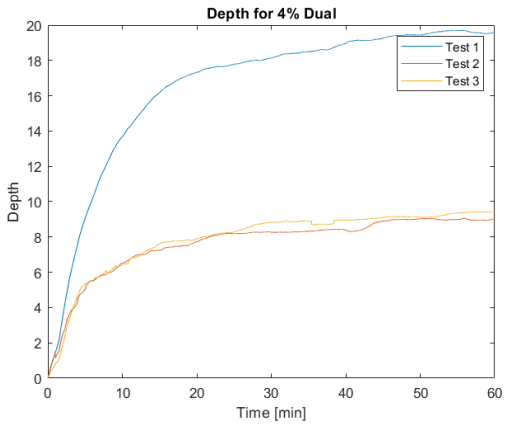


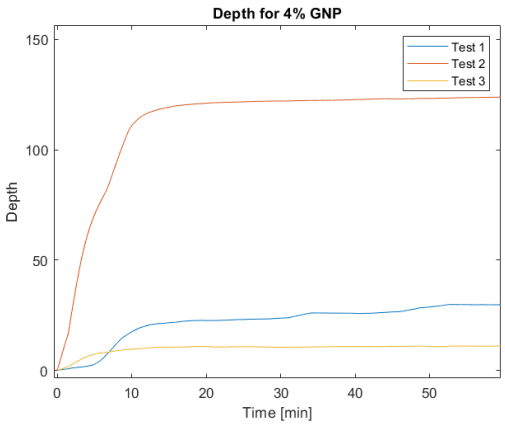

THIS PAGE INTENTIONALLY LEFT BLANK

# LIST OF REFERENCES


[1] U.S. Department of Defense, "Manufacturing process standard: Materials deposition, Cold Spray. MIL-STD-3021." Army – MR, Jul. 13, 2011 [Online]. Available: http://everyspec.com/MIL-STD/MIL-STD-3000-9999/MIL-STD-3021_CHG-2_52134/

[2] P. F. Leyman and V. K. Champagne, "Cold spray process development for the reclamation of the apache helicopter mast support," Army Research Laboratory, Aberdeen, MD. Accessed: Apr. 13, 2023 [Online]. Available: https://apps.dtic.mil/sti/citations/ADA505530

[3] J. K. Bi, Z. C. K. Loke, C. K. R. Lim, K. H. T. Teng, and P. K. Koh, "Mechanical properties of cold sprayed aluminium 2024 and 7075 coatings for repairs," *Aerospace*, vol. 9, no. 2, Art. no. 2, Feb. 2022, doi: 10.3390/aerospace9020065.

[4] M. M. Sharma, T. J. Eden, and B. T. Golesich, "Effect of surface preparation on the microstructure, adhesion, and tensile properties of cold-sprayed aluminum coatings on AA2024 substrates," *J. Therm. Spray Technol.*, vol. 24, no. 3, pp. 410–422, Feb. 2015, doi: 10.1007/s11666-014-0175-1.

[5] S. P. Rice, "Enhancing mechanical properties of cold-sprayed aluminum coatings using graphene-nanoplatelet and micro-boron-carbide reinforcements," Thesis, Monterey, CA; MAE Dept, Naval Postgraduate School, 2022. Accessed: Nov. 17, 2022 [Online]. Available: https://calhoun.nps.edu/handle/10945/70729

[6] CenterLine SST, "CenterLine Supersonic Spray Technology – How it Works" [Online]. https://www.supersonicspray.com/innovation-technology/how-it-works (accessed Nov. 16, 2022).

[7] T. Stoltenhoff, H. Kreye, and H. J. Richter, "An analysis of the cold spray process and its coatings," *J. Therm. Spray Technol.*, vol. 11, no. 4, pp. 542–550, Dec. 2002, doi: 10.1361/105996302770348682.

[8] M. Grujicic, C. L. Zhao, C. Tong, W. S. DeRosset, and D. Helfritch, "Analysis of the impact velocity of powder particles in the cold-gas dynamic-spray process," *Mater. Sci. Eng. A*, vol. 368, no. 1, pp. 222–230, Mar. 2004, doi: 10.1016/j.msea.2003.10.312.

[9] M. Ashokkumar, D. Thirumalaikumarasamy, T. Sonar, S. Deepak, P. Vignesh, and M. Anbarasu, "An overview of cold spray coating in additive manufacturing, component repairing and other engineering applications," *J. Mech. Behav. Mater.*, vol. 31, no. 1, pp. 514–534, Jan. 2022, doi: 10.1515/jmbm-2022-0056.

[10] S. Singh, R. Raman, C. Berndt, and H. Singh, "Influence of cold spray parameters on bonding mechanisms: A review," *Metals*, vol. 11, p. 2016, Dec. 2021, doi: 10.3390/met11122016.

[11] S. Ngai, T. Ngai, F. Vogel, W. Story, G. B. Thompson, and L. N. Brewer, "Saltwater corrosion behavior of cold sprayed AA7075 aluminum alloy coatings," *Corros. Sci.*, vol. 130, pp. 231–240, Jan. 2018, doi: 10.1016/j.corsci.2017.10.033.

[12] T. Schmidt, F. Gaertner, and H. Kreye, "New developments in cold spray based on higher gas and particle temperatures," *J. Therm. Spray Technol.*, vol. 15, no. 4, pp. 488–494, Dec. 2006, doi: 10.1361/105996306X147144.

[13] P. C. King and M. Jahedi, "Relationship between particle size and deformation in the cold spray process," *Appl. Surf. Sci.*, vol. 256, no. 6, pp. 1735–1738, Jan. 2010, doi: 10.1016/j.apsusc.2009.09.104.

[14] B. Jodoin, L. Ajdelsztajn, E. Sansoucy, A. Zúñiga, P. Richer, and E. J. Lavernia, "Effect of particle size, morphology, and hardness on cold gas dynamic sprayed aluminum alloy coatings," *Surf. Coat. Technol.*, vol. 201, no. 6, pp. 3422–3429, Dec. 2006, doi: 10.1016/j.surfcoat.2006.07.232.

[15] D. A. Rigney, "Comments on the sliding wear of metals," *Tribol. Int.*, vol. 30, no. 5, pp. 361–367, May 1997, doi: 10.1016/S0301-679X(96)00065-5.

[16] D. Lahiri *et al.*, "Cold sprayed aluminum based glassy coating: Synthesis, wear and corrosion properties," *Surf. Coat. Technol.*, vol. 232, pp. 33–40, Oct. 2013, doi: 10.1016/j.surfcoat.2013.04.049.

[17] X. Xie *et al.*, "Corrosion behavior of cold sprayed 7075Al composite coating reinforced with TiB2 nanoparticles," *Surf. Coat. Technol.*, vol. 404, p. 126460, Dec. 2020, doi: 10.1016/j.surfcoat.2020.126460.

[18] M. Imran and A. R. A. Khan, "Characterization of Al-7075 metal matrix composites: A review," *J. Mater. Res. Technol.*, vol. 8, no. 3, pp. 3347–3356, May 2019, doi: 10.1016/j.jmrt.2017.10.012.

[19] Valimet, "Additive manufacturing aluminum alloy powders" [Online]. https://valimet.com/additive-manufacturing-aluminum-alloy-powders/ (accessed Jan. 20, 2023).

[20] Y. Liu, J. M. C. Mol, and G. C. A. M. Janssen, "Combined corrosion and wear of aluminium alloy 7075-T6," *J. Bio- Tribo-Corros.*, vol. 2, no. 2, p. 9, Apr. 2016, doi: 10.1007/s40735-016-0042-3.

[21] O. Meydanoglu, B. Jodoin, and E. S. Kayali, "Microstructure, mechanical properties and corrosion performance of 7075 Al matrix ceramic particle reinforced composite coatings produced by the cold gas dynamic spraying process," *Surf. Coat. Technol.*, vol. 235, pp. 108–116, Nov. 2013, doi: 10.1016/j.surfcoat.2013.07.020.

[22] U.S. Research Nanomaterials, "Boron carbide powder / B4C powder (B4C, 99.9%)" [Online]. https://www.us-nano.com/inc/sdetail/6703 (accessed Jan. 10, 2023).

[23] V. Domnich, S. Reynaud, R. A. Haber, and M. Chhowalla, "Boron carbide: Structure, properties, and stability under stress," *J. Am. Ceram. Soc.*, vol. 94, no. 11, pp. 3605–3628, Nov. 2011, doi: 10.1111/j.1551-2916.2011.04865.x.

[24] A. Nieto, H. Yang, L. Jiang, and J. M. Schoenung, "Reinforcement size effects on the abrasive wear of boron carbide reinforced aluminum composites," *Wear*, vol. 390–391, pp. 228–235, Nov. 2017, doi: 10.1016/j.wear.2017.08.002.

[25] A. Jiménez-Suárez and S. G. Prolongo, "Graphene nanoplatelets," *Appl. Sci.*, vol. 10, no. 5, Art. no. 5, Jan. 2020, doi: 10.3390/app10051753.

[26] U.S. Research Nanomaterials, "Graphene nanoplatelets / graphene nanoPowder (95+%, Thickness 2–8nm, 3–6 layers)" [Online]. https://www.us-nano.com/inc/sdetail/18480 (accessed Jan. 10, 2023).

[27] A. Nieto, A. Bisht, D. Lahiri, C. Zhang, and A. Agarwal, "Graphene reinforced metal and ceramic matrix composites: A review," *Int. Mater. Rev.*, vol. 62, no. 5, pp. 241–302, Jul. 2017, doi: 10.1080/09506608.2016.1219481.

[28] T. Y. Ansell, T. Hanneman, A. Gonzalez-Perez, C. Park, and A. Nieto, "Effect of high energy ball milling on spherical metallic powder particulates for additive manufacturing," *Part. Sci. Technol.*, vol. 39, no. 8, pp. 981–989, Nov. 2021, doi: 10.1080/02726351.2021.1876192.

[29] SPEX SamplePrep, "8000D MixerMill manual" [Online]. https://www.spexsampleprep.com/knowledge-base/resources/manuals/8000D%20MixerMill%20Manual%20100714%20abridged.pdf

[30] Associated Environmental Systems, "MX-9204" [Online]. https://www.associatedenvironmentalsystems.com/products/MX-9204 (accessed Jan. 25, 2023).

[31] Nanovea, "Standard modular tribometer T50," *NANOVEA* [Online]. https://nanovea.com/instruments/t50/ (accessed Feb. 07, 2023).

[32] Struers, "Secotom precision cutting machine" [Online]. https://www.struers.com/en/Products/Cutting/Cutting-equipment/Secotom# (accessed Feb. 06, 2023).

[33] A. Fardan, C. C. Berndt, and R. Ahmed, “Numerical modelling of particle impact and residual stresses in cold sprayed coatings: A review,” *Surf. Coat. Technol.*, vol. 409, p. 126835, Mar. 2021, doi: 10.1016/j.surfcoat.2021.126835.

# INITIAL DISTRIBUTION LIST

1. Defense Technical Information Center
   Ft. Belvoir, Virginia

2. Dudley Knox Library
   Naval Postgraduate School
   Monterey, California